Studies of Ferric Heme Proteins with Highly Anisotropic/Highly Axial Low Spin (S=1/2) Electron Paramagnetic Resonance Signals with bis-Histidine and Histidine-Methionine Axial Iron Coordination

Zoppellaro, Giorgio; Bren, Kara L.; Ensign, Amy A.; Harbitz, Espen; Kaur, Ravinder; Hersleth, Hans-Petter; Ryde, Ulf; Hederstedt, Lars; Andersson, K. Kristoffer

Published in:
Biopolymers

DOI:
10.1002/bip.21267

2009

Document Version:
Peer reviewed version (aka post-print)

Studies of ferric heme proteins with Highly Anisotropic/Highly Axial Low Spin (S = 1/2) electron paramagnetic resonance signals with two histidines or histidine and methionine axial Fe coordination.

In honor of Professor Lelio Mazzarella

Giorgio Zoppellaro[1], Kara L. Bren[2], Amy A. Ensign[2], Espen Harbitz[1], Ravinder Kaur[2], Hans–Petter Hersleth[1], Ulf Ryde[3], Lars Hederstedt[4] and K. Kristoffer Andersson[1*]

Affiliations: Oslo, Rochester, Lund,
[1]Department of Molecular Biosciences, University of Oslo, PO Box 1041 Blindern, Oslo NO0316, Norway
[2]Department of Chemistry, University of Rochester, Rochester, New York 146270216, USA
[3]Department Theoretical Chemistry, Lund University, Chemical Centre, P. O. Box 124, SE–221 00 Lund, Sweden
[4]Department of Cell & Organism Biology, Lund University, Sölvegatan 35, SE–22362 Lund, Sweden

Keywords: Cytochrome, DFT calculation, EPR, ^{1}H NMR, ligand–field anisotropy

Correspondence to: K. Kristoffer Andersson, k.k.andersson@imbv.uio.no ,

Phone: +47-22856625; Fax: +47-22856041

Contract grant sponsor/Contract grant number:

This work was supported by the Research Council of Norway Grant 177661/V30 (K.K.A.) and Grant 157855 (E.H., and K.K.A.), and from The National Institute of Health (NIH) of the United States of America Grant GM63170 (R.K., A.A.E. and K.L.B.) to Kara Bren.

Research in the Lars Hederstedt and Ulf Ryde groups were supported by the Swedish Research Council.

ABSTRACT

Six–coordinated heme groups are involved in a large variety of electron transfer reactions because of their ability to exist in both the ferrous (Fe^{2+}) and ferric (Fe^{3+}) state without any large differences in structure. Our studies on hemes coordinated by two histidines (bis–His) and hemes coordinated by histidine and methionine (His–Met) will be reviewed. In both of these coordination environment, the heme core can exhibit ferric low spin EPR signal with large g_{max} values (also called type I, highly anisotropic low spin, or highly axial low spin, HALS species) as well as rhombic EPR (type II) signals. In bis–His coordinated hemes rhombic and HALS envelopes are associated to the orientation of the His groups with respect to each other such that (i) parallel His planes results in rhombic signal and (ii) perpendicular His planes results in HALS signal. Correlation between the heme structure with His and Met axial ligation and ligand–field parameters, as derived from a large series of cytochrome *c* over-expressed proteins and mutants, show however that for such combination of axial ligand there is no clear–cut difference between the large g_{max} and the "small *g*–anisotropy" cases as a result of the relative Met–His arrangements. Nonetheless, a new correlation was found that link the averaged shift $<\delta>$ of the heme methyl hydrogens with the g_{max} values.

INTRODUCTION

The iron containing heme group is found in all parts of biology and carries out a great diversity of functions.[1,2] The ability of the iron atom to exist in different oxidation states makes it ideal for functions like oxygen transport and storage (myoglobin and hemoglobin), catalysis (e.g. cytochrome P–450[3], hydroxylamine oxidoreductase[4] with 24 hemes) and electron transfer. From the structural perspective, the Fe metal ion in a hemeprotein is always coordinated by four nitrogen atoms provided by a porphyrin ring embedded in the protein core. Heme proteins involved in catalysis, oxygen transport or storage have an amino acid as one axial ligand to the iron, which is either five-coordinated or has a water molecule at (or close to) the sixth coordination site in the resting state (Hersleth *et al.*).[5-7] Some of these proteins can have a substrate(s) and oxygen/peroxide binding pocket accessible to the heme iron. Heme proteins that perform electron transfer reactions usually have both axial ligands donated by amino acid residues with the exception of some cytochromes *c*' that have unknown function.[8,9] The most common biologically relevant axial ligating atoms for Fe are nitrogen in histidine (His) residues (possibly lysine) or the polypeptide N−terminal amino group, sulfur in Met or cysteine groups, and oxygen in tyrosine. Cytochromes are essential components in all organisms that posses a respiratory chain or a photosynthetic system, and in prokaryotes, because they can act as electron–transfer proteins within cellular metabolism or have catalytic function. Different types of such proteins have been discovered in Nature from the time when McMunn in 1886 described the colored substances in cells,[10] addressed later on by Keilin with the term "cytochrome".[11] Cytochromes and heme proteins can be divided into classes according to the heme type (e.g., *a*, *b*, *c*, *d*, *f*, and *o*), heme iron coordination environment (e.g. heme *a* and a_3) and sequence homologies. The Fe metal ion in both oxidized (+3) and reduced (+2) states adopts a low–spin configuration (S = ½ and S = 0 respectively) in cytochromes while in other heme proteins several different spin and redox states are possible. Therefore in

cytochromes only the oxidation state of the metal changes, thus minimizing the reorganization energy associated with the electron transfer processes.[12] Combination of spectroscopic techniques like EPR (X-band or HF-EPR, ENDOR, HYSCORE and ESEEM), Mössbauer, XAS, resonance Raman, IR, NMR and MCD, complemented by theoretical calculations and structural analyses (X–ray diffraction) aim to relate protein structure, electronic and magnetic properties to the protein function. Especially when structural information is absent, the spectroscopic fingerprints of the heme proteins can be used as blueprints to disclose the nature of heme axial ligands, their mutual orientation and dynamics with respect to the heme core.[13] Here we summarize how and to what extent the ferric ligand field anisotropy is modulated in two cytochrome classes, those encompassing coordination with two His residues and those having methionine (Met) and His (*c*–type cytochromes) as axial ligands. For both of these two types of coordination sets we see a low spin ferric (Fe^{3+}) EPR signals with large g_{max} and/or normal rhombic spectra. The covalent attachment of the heme group in *c*–type heme proteins does not in general alter very much the reduction potential, but it is required to ensure the high thermodynamic stability.[14] The edge of the heme group is often solvent exposed and surrounded by amino acids which are complementary to their partner proteins. The covalent attachment guarantees that the heme group is retained in the protein and might help to fix the position.[15-17] Correlation of structures with the observed electronic and magnetic properties of the heme group show that for the bis–His heme proteins, the protein structural architecture, such as the relative orientation of the axial ligands and/or highly saddled–shaped versus ruffled heme plane, represent the dominating factors responsible for tuning the Fe ligand field. On the contrary, for cytochromes *c* with Met and His coordinated to heme iron, a clear assessment of the factors that steer the ligand–field strength are still unclear, since even small perturbations in one of the axial ligand (Met) induce alteration of the heme ligand field anisotropy (see for instance recent reviews by Bowman and Bren[18] for cytochromes *c* and

Berry and Walker[19] for bis–His proteins). Therefore better understanding how the Fe electronic configuration is modulated by the heme surrounding and then how much those effects contribute to alter the heme ligand field anisotropy will help to pave the way to uncover the subtleties that govern electronic structure and reactivity in this important class of molecule.

LIGAND FIELD ANISOTROPY IN LOW–SPIN HEME IRON

In a low–spin ferric heme system,[20] the electronic ground state of the heme core is modulated by the effect of the crystal field acting on the d^5 configuration[21] of the ferric metal ion. Analyses of the protein molecular structure, when available, in combination with spectroscopic techniques such as electron paramagnetic resonance (EPR), nuclear magnetic resonance (NMR), near IR–MCD, vibrational techniques and in some cases with the aid of Mössbauer analyses, demonstrate that low–spin cytochromes having a $(d_{xy})^2(d_{xz})^2(d_{yz})^1$ orbital occupancy can mainly exhibit two very different type of ground state electronic configurations, but F. Ann Walker has suggested more types.[22] These differences are expressed in terms of crystal field parameters, rhombic (V) and axial (Δ), which follow the formalism introduced by Griffith[23] and developed by Taylor[24] (Figure 1). However, depending on the strength of the rhombic versus axial field (V/Δ), the heme core can experience the whole spectrum of intermediate axial versus rhombic strained configurations, as shown in Figure 2 and Figure 3 for a set of representative EPR envelopes recorded in cytochrome proteins. Under this formalism, and with the assumption that the following limiting conditions hold, $V \rightarrow 0$ for a completely axial system, and $V/\Delta = 0.67$ for a pure rhombic system[25], the difference in the ligand–field strengths between axial ligands and porphyrin ligands induces the splitting in energy of the three t_{2g} orbitals (d_{yx}, d_{xz} and d_{yz}). The unpaired electron in the low–spin Fe^{3+} is thus located in a new orbital described as an admixture of the former three t_{2g}

orbitals through the spin–orbit coupling factor (ξ). The wavefunctions for the Kramer's doublet are then given by Eq. (1) and (2), where a, b and c are orbital coefficients:

$$|+> = a\,|\,d_{yz}^{+}> - ib|\,d_{xz}^{+}> - c\,|\,d_{xy}^{-}> \quad (1)$$

$$|-> = -a\,|\,d_{yz}^{-}> - ib\,|\,d_{xz}^{-}> - c\,|\,d_{xy}^{+}> \quad (2)$$

According to Taylor's treatment, equation (1) and (2) are valid as long as the remaining two empty e_g orbitals ($|d_{x^2-y^2}>$ and $|d_{z^2}>$) lie sufficiently high in energy such that their contributions can be neglected. The g–tensor values experimentally found are then correlated with the mixing coefficients a, b and c through the following expressions:

$$g_{xx} = 2\,[\,a^2 - (b + c)^2]$$

$$g_{yy} = 2\,[-b^2 + (a + c)^2]$$

$$g_{zz} = 2\,[-c^2 + (a + b)^2] \quad (3)$$

Where

$$a^2 + b^2 + c^2 \equiv 1$$

In particular, the sum of the squared coefficients (a, b, c) is strictly equal to "one" only when the pure ionic (no covalency) orbital character is considered. The g–tensor values are related to each other through Eq. (4):

$$g_{xx}^{\,2} + g_{yy}^{\,2} + g_{zz}^{\,2} + g_y g_z - g_x g_z - g_x g_y - 4(g_{zz} + g_{yy} - g_{xx}) = 0 \quad (4)$$

The crystal field parameters V/ξ and Δ/ξ are then calculated from the g–tensor values according to Eq. (5) and (6):

$$\frac{V}{x} = \frac{E_{yz}}{x} - \frac{E_{xz}}{x} = \frac{g_{xx}}{g_{zz} + g_{yy}} + \frac{g_{yy}}{g_{zz} - g_{xx}} \quad (5)$$

$$\frac{\Delta}{x} = \frac{E_{yz}}{x} - \frac{E_{xy}}{x} - \frac{V}{2x} = \frac{g_{xx}}{g_{zz} + g_{yy}} + \frac{g_{zz}}{g_{yy} - g_{xx}} - \frac{V}{2x} \quad (6)$$

where V is the energy difference between the d_{xz} and d_{yz} orbitals, Δ the difference between the d_{xy} and the averaged energy of the d_{xz} and d_{yz} orbitals and ξ the spin orbit coupling constant (~

400 cm^{-1}).[26,27] The knowledge of all three g values is therefore necessary in order to determine V/ξ and Δ/ξ. However, in many cases experimental observation of the g_{xx} (or g_{min}) component is difficult, because it falls at high field and is usually broad and weak. Therefore equation (4) can be used to calculate g_{xx} when g_{zz} (g_{max}) and g_{yy} (g_{mid}) are known. Another relationship similar to equation (4) is that $(g_{xx})^2 + (g_{zz})^2 + (g_{yy})^2 = 16$ holds in many cases, but especially for EPR of large g_{max} it might not be true, as discussed by Gadsby and Thomson.[28] The complication concealed in Eq. (4) is that the EPR measurements can provide only the magnitude but not the g–tensor signs.[25,29] Two different solutions in term of crystal field parameters can be obtained, which correspond to a very different unpaired electron distribution. However, one constraint is to consider that the sum $[g_{zz} + g_{yy} - g_{xx}]$ needs to be positive,[24] and this additional condition limits the number of possible choices of signs for g. Huynh and coworkers[30] demonstrated that the product of the three principal g–tensor values was positive in the case of cytochrome c_2 from *Rhodospirillum rubrum* through Mössbauer analyses. We have also observed the same positive g–tensor product in the cytochrome *Nitrosomonas europaea c*–552, which exhibits large g_{max} value.[31] Therefore it is likely that for similar cytochromes this constitutes a "general case". Eq. (4) fails when residual contributions from higher excited states are not negligible and this seems to become relevant in the high temperature regime, or when the systems shift from fairly pure $(d_{xy})^2(d_{xz})^2(d_{yz})^1$ ground state to a fairly pure $(d_{xz})^2(d_{yz})^2(d_{xy})^1$ ground state,[32-35] or finally in the absence of efficient spin–orbit ξ mixing among the t_{2g} orbitals.

APPLICATION OF EPR SPECTROSCOPY TO THE ANALYSES OF LOW–SPIN HEME IRON

Since the early work of Blumberg and Peisach in the 1970s,[13,36] EPR spectroscopy has been used widely to classify low–spin Fe^{3+} heme in terms of axial ligands bound to the heme core by analyses of their crystal–field parameters.[20] Looking at the different set of EPR *g*–resonances experimentally observed in several low spin cytochomes, such as those shown for example in Figure 2 and Figure 3, two prototypical patterns emerge that mirror the two limiting ground state configurations possible for the low–spin Fe^{3+} ion, as described in the Griffith and Taylor's formalism. Type I heme (Figure 2 A, C and D and Figure 3 A–D), according with the nomenclature introduced by Walker,[29] are characterized by near degeneracy between d_{xz} and d_{yz} orbitals, with energy difference ΔE (with $\Delta E = E(d_{yz}) - E(d_{xz})$) smaller than the spin–orbit coupling constant (ξ). In this scenario, the EPR spectrum exhibits large *g*–anisotropy, with $g_{max} > 3.3$ and g_{mid}, g_{min} rather small and broad.[37-39] Here the rhombic parameter *V* is small (e.g. ~1.0 ξ in cyt *c* with His–Met axial ligands, 0.28 ξ in the Mb–CN complex)[28,29] with limiting value zero. Type I heme are also referred in literature to as highly anisotropic low spin heme[40,41] or highly axial low spin heme (HALS).[39] In these systems the EPR envelopes are typically observed only at cryogenic temperatures (< 30 K). In addition the g_{max} resonance line can be either Gaussian–like (e.g. Figure 3D) or highly asymmetric (e.g. Figure 2A and 2C), which is observed especially for membrane bound proteins with bis–His iron coordination. The heme *b* with g_{max} at 3.7 (Figure 2C) is very similar to the heme b_L from complex III in mitochondria.[42] The origin of such different behaviour is still matter of controversy; the line–shape asymmetry has been interpreted either due to the presence of multiple components (DeVries and Albracht)[37] or arising from *g*–strain effects, that are regarded as micro–heterogeneities in the protein conformation occurring upon

freezing (Salerno).[39] When a large energy difference ΔE between the d_{xz} and d_{yz} orbitals is present, up to three times ξ (between 600–1200 cm^{-1}),[27] all three g values (g_{max}, g_{mid} and g_{min}) can be resolved in the spectrum which are characterized by smaller g–anisotropy ($g_{max} < 3.2$). Furthermore the EPR resonance line can be observed at higher temperatures as compared to type I heme, sometimes up to liquid nitrogen, especially with proteins containing thiolate axial coordination. In this case the heme is called type II or rhombic (Figure 2B), and the ratio V/Δ approaches the theoretical limiting value 0.67 (Figure 3I). Highly axial low–spin EPR spectra have been observed in several different classes of cytochromes. These include membrane bound *b*–type proteins (bis-His axial ligands), such as the two hemes of cytochrome b_{558} (in succinate dehydrogenase, succinate:quinone reductase) from *Bacillus subtilis,*[43,44] analogous to Complex II of the bovine mitochondrial respiratory chain (see below), cytochrome b_{562} and b_{566} in Complex III of the bovine mitochondrial respiratory chain (complex bc_1),[45,46] and in one of the three hemes from the multi–subunit cytochrome *bf* complex.[47,48] HALS EPR signals are also observed in the myoglobin $His^{64}\rightarrow Val/Val^{68}\rightarrow His$ double mutant protein,[49] in horse cytochrome *c*–CN complex,[28] cytochrome *c* peroxidase from *Nitrosomonas europaea* (His and Met)[50] and cytochrome *c*–553 from *Bacillus pasteurii* (His and Met) (Figure 3D).[31] A similar envelope is exhibited by cytochrome *c*–552 from *Nitrosomonas europaea* [51](*Ne c*–552; His and Met) (Figure 2A and Figure 3B), in some of its mutants such as NeV65Δ (Figure 3C) and NeG50N/V65Δ (Δ indicates the amino acid deletion, spectrum not shown)[52] and in cytochrome *c*–554 OB3b from *Methylosinus trichosporium* (Figure 3A)[53] while the *Metylococcus capsulatus bath* cytochrome *c*–555 has rhombic EPR signal (Figure 3I). [54,55]

DETERMINATION OF AXIAL LIGANDS IN HEME–PROTEINS THAT EXHIBITS HALS SIGNAL. EXAMPLES OF BIS–HIS LIGANDS.

An observed ferric low spin large g_{max}/HALS/type EPR spectrum for an otherwise little characterized heme–protein does not provide much information on the nature of the two axial ligands to the heme iron atom. For example, at the time when little molecular data was available for the cytochrome *b*–558 subunit of *Bacillus subtilis* succinate:menaquinone reductase, we described large g_{max}–type low spin EPR signals from the two *b*–hemes.[44] The broadness of the signals with g_{max} at 3.38 and 3.46 for the respective hemes (Table 1) makes them difficult to detect compared to heme signals with g_{max} = around 3.0 and usually only the g_{max} can be observed.[56] In addition to that, quantification of HALS/type I Fe(3+) heme is also complicated in some cases, as shown for example by the cytochrome b_6f complex where one of the heme group was "missed" and which could be identified only after the 3D structure became known and the heme–heme interacting pair could be observed through integer spin EPR detection technique.[48] One useful spectroscopic approach to retrieve information about possible axial ligands to heme iron is to combine EPR with near–infrared magnetic circular dichroism (NIR–MCD) at low temperatures. Different combinations of axial heme ligands give characteristic near NIR–MCD spectra.[28] The two hemes in *B. subtilis* SQR showed at 4.2 K and 5 Tesla an intense NIR–MCD charge transfer band at 1600 nm[43] typical of bis–His ligation and near perpendicular orientation of the imidazole planes. Membrane–bound succinate:fumarate oxidoreductases, i.e., succinate:quinone reductases (SQRs) and fumarate:quinol reductases QFRs), in different organisms are rather unique among respiratory proteins in that the membrane–extrinsic part is very conserved in amino acid sequence, prosthetic group composition and three–dimensional structure whereas the membrane–intrinsic part shows extensive diversity.[57] The membrane–extrinsic part harbors the enzyme dicarboxylic acid binding active site and consists of a flavoprotein and an iron–sulfur protein.

The membrane intrinsic part functions to anchor the extrinsic–part to the membrane and is important for quinone oxidation/reduction. It consists of one or two polypeptides with 5 or 6 transmembrane segments and contains one or two low spin hemes or lacks heme. For example, *E. coli* SQR and QFR both have two anchor polypeptides with 3 transmembrane segments each but only SQR contains heme (Table 1). Mammalian, avian and yeast mitochondrial SQR is similar to *E. coli* SQR. *B. subtilis* SQR and *Wolinella succinogenes* QFR contain one polypeptide with 5 transmembrane segments and two heme *b* groups. Comparative studies indicate that the anchor parts of all SQRs and QFRs are homologous, i.e. that they have evolved from two–polypeptide primordial variant containing two hemes.[58] Based on a combined use of redox–coupled spectroscopic analysis (light absorption, EPR and NIR–MCD), well defined mutant variants, and the identification of invariant residues by multiple amino acid sequence comparisons, a three–dimensional model structure of the membrane–integral part of *B. subtilis* SQR was elucidated.[59] Identification of the His residues acting as the axial ligands to the respective heme and the distribution of these four residues on four different transmembrane segments served as keys in the formulation of the model. Three–dimensional atomic crystal structures are now available for several SQRs and QFRs from different organisms. The structural data demonstrate bis–His axial ligation of heme–iron in all cases where heme is present (Figure 4 panel C with avian SQR) and confirm the arrangement of heme within a four–helix bundle as originally proposed in the model. As in most other cytochromes, the N(3) atom of the imidazole ring binds the iron atom. The structures also confirm near perpendicular orientation of the planes of the two ligating imidazole groups as originally indicated by EPR combined with low temperature NIR–MCD spectroscopy. The mode of binding of menaquinone to diheme SQR or QFR and the mechanism of menaquinone reduction/oxidation by these enzymes have not been elucidated. For the *B. subtilis* SQR, menaquinone it is thought to be reduced in proximity to the distal

heme (b_D) group located close to the outer side of the cytoplasmic membrane.[60-62] Electron transfer from the proximal heme (b_P), which has a high midpoint redox potential and is located close to the membrane–extrinsic part of the enzyme on the inner (cytoplasmic) side of the membrane, to heme b_D (which has a low mid–point potential) is believed to be driven by the transmembrane electrochemical potential. 2–n–heptyl–4–hydroxyquinoline–N–oxide (HQNO) is a mena–semiquinone analogue that binds to the membrane part of *B. subtilis* SQR and inhibits menaquinone reduction.[63] Binding of HQNO shifts the g_{max} in the EPR spectrum of heme b_D and also causes a negative shift in the redox potential of that heme.[62] Residues His28 and His113 ligate heme b_D.[59,64] Experimental results from studies with His28 and His113 single substitution mutant variants and pseudo–revertants obtained with these mutants show that a Met residue at position 113 is functional, probably as the result of His–Met axial ligation of heme b_D in the mutant.[62] An increased midpoint redox potential of heme b_D in that mutant compared to wild type is consistent with a change from bis–His to His–Met axial ligation.[62]The His113Met variant reduces menaquinone and binds HQNO. The properties of heme in the His28L variant are seemingly not affected by HQNO and pseudo–revertants could not be found by selection indicating that a His28Met enzyme variant does not assemble properly or is enzymatically inactive. Similar to *B. subtilis* SQR, the membrane–integral part of *E. coli* formate dehydrogenase–N (FDH–N) contains two hemes *b* with bis–His axial ligation. In the crystal structure of FDH–N one molecule of added HQNO was found close to one of the axial ligands (His169) of the distal heme.[65] The porphyrin ring of the heme was seen in van der Waals contact with the hydroxyquinoline N–oxide ring and the N–oxide group of HQNO (corresponding to O_1 of menaquinone) accept a hydrogen bond to the N(1) atom of the imidazole group His169. In analogy, it is possible that N(1) of the imidazole group of residue His28 in the membrane–intrinsic polypeptide of *B. subtilis* SQR via a hydrogen bond directly ligates menaquinone (and HQNO) while the N(3) atom ligates the heme b_D iron atom.

This would explain why functional His28Met pseudo–revertants could not be found; the sulphur atom of the Met binds to heme iron and cannot properly ligate menaquinone which renders the enzyme inactive. Another example involving a quinol model hydrogen-bonding to SQR and FDH–N, analogous to the N(1), is illustrated in the drawings reported in Figure 4A and 4B, which show the effects induced by the presence of the inhibitor pentachlorophenol (PCP).[66] One possible role of some of the membrane–bound HALS–containing proteins that reacts with a quinone/quinol pair could be that the perpendicular His configuration could facilitate reactions with the quinone/quinol residue. In fact, the HALS signal increases (g_{max} shifts from 3.35 to 3.45 or 3.50) upon binding a quinol analogue or the natural quinol, in *Escherichia coli* nitrate reductase A. In order to examine if such changes arise from significant perturbation of the electronic configuration of the heme or axial ligand core, we have used density functional theory (DFT) calculations based on the known crystal structure of *E. coli* nitrate reductase A (Table 2 and Figure 5). However, as Figure 5 shows, we could not observe any significant differences in the spin density distribution within by the heme core with or without inhibitor (PCP) or phenol (Table 2) groups.

LIGAND FIELD ANISOTROPY IN HEME *A* SYNTHASE (HAS)

Heme *a* synthase is so far the only example of a protein with a ferric low spin large g_{max}/HALS/type signal at g_{max} = 3.5 (Figure 2D) from ligated heme *a*.[67] Heme *a* differs from heme *b* in that there is a hydroxylethyl–prenyl side group at position 2 of the porphyrin ring and a formyl group at position 8. As a prosthetic group, heme *a* is only found in terminal respiratory enzymes that reduce molecular oxygen to water, i.e. in *a*–type cytochromes. HAS catalyses the conversion of the methyl side group of heme *o* into a formyl group yielding heme *a*.[68] This reaction is formally an oxygenation and dehydrogenation reaction which on the enzyme is believed to occur in three steps; two sequential monooxygenations resulting in

a vicinal dihydroxy intermediate that in the third step spontaneously is dehydrated to form heme *a*.[69,70] *B. subtilis* HAS (CtaA) purified from recombinant *E. coli* or overproduced in *B. subtilis* cells contains heme *b* and different (depending on production strain) amounts of heme *a*.[67] Also HAS of *Aeropyrum pernix* (a hyperthermophilic bacterium) produced in *E. coli* contains heme *b* and *a*.[71] The bound heme *a* is an enzyme product that has not been released from the enzyme due to lack of accepting proteins, i.e., apo–cytochrome *a* polypeptides. Heme *b* in HAS either functions as a prosthetic group or is an artifact caused by the experimental systems where in all cases the protein is overproduced. Both heme *a* and heme *b* in HAS show low–spin EPR signals, with g_{max} at 3.5 and 3.7, respectively.[67] HAS is an integral membrane protein with several invariant His residues distributed on different transmembrane segments. Three of these residues (His60, His123 and His216 in *B. subtilis* CtaA) are important for activity as determined from studies with mutant protein variants.[70,72] Based on available data it is thought that heme *b* and heme *a* in HAS have bis–His ligation, but this needs to be established using low temperature NIR–MCD and ultimately crystal or NMR structural analysis.

BIS–HIS VERSUS MET–HIS HEME COORDINATIONATION. HOW STRUCTURAL FACTORS MODULATE THE HEME ELECTRONIC PROPERTIES.

The correlations between EPR axial strain and axial ligand arrangements have been extensively investigated and well rationalized over the years for *b*–type cytochromes with bis–His heme axial ligation as well as for several of their mimicking complexes.[22,29] In this type of heme group, HALS–type EPR spectra arise as a result of the mutual perpendicular orientation of the axial imidazole ligands (intra–ligand plane angle ~70˚–90˚) which induces a small rhombic distortion V/ξ. Hemes with an angle between two axial imidazole planes of less than 70˚ display rhombic EPR spectra.[22] Furthermore, correlation of the protein structure

and/or synthetic model molecular structures with the observed electronic properties of the heme group shows that also other aspects contribute to modulating the ligand–field strength. Those can be summarized as following: (i) the presence of strong axial ligands (strong σ–donors and weak π–acceptors) combined with (ii) a highly saddled–shaped heme plane, and/or (iii) electron withdrawing groups attached at the meso positions of the porphyrin cause the heme configuration to be stabilized towards the axial $(d_{xy})^2(d_{xz},d_{yz})^3$ state. In cytochromes *c* having Met and His coordinated to heme iron, however, assessment of the leading factors that steer the ligand–field strength is unfortunately not so clear. A throughout analyses of those factors will provide crucial information for better understanding the correlation between structure/electronic properties/function of the membrane–bound cytochrome c_1 in the mitochondrial complex III, as well as many small and multiheme soluble proteins.[39,73]

The two *b*–hemes in *B. subtilis* cytochrome *b*–558 exhibit at 4.2 K and 5 Tesla an intense charge–transfer NIR–MCD at 1600 nm which is typical of near perpendicular orientation of the His planes, while the *N. europaea c*–552 with His–Met coordination features an intense charge–transfer band at 1800 nm.[51] NIR–MCD can also detect other combination of axial ligand, including unusual ones like bis–Met at 2200 nm.[74] Met coordination to hemes shows as a fingerprint the typical weak ferric optical band around 690–710 nm. Iron coordination with sulphur has larger involvement of covalent binding, therefore Mössbauer spectroscopy in combination with EPR analyses can be used to clearly asses the *g*–tensor and *A*–tensor parameters, as we earlier had shown for Ne–552.[31] In Figure 6 and 7 are shown typical structures of His–Met coordinated cytochromes *c*, of which EPR spectra are discussed in this review. Figure 7 in particular, shows the location of mutations of Ne–552 and Pa–551 with corresponding EPR spectra illustrated in Figure 3. From a structural perspective, the mitochondrial cytochromes *c* have an intra–ligand angle (measured as the angle between the π nodal planes of the His and Met) of ~48˚ and display rhombic EPR spectra (g_{max} ~ 3.1 and

V/Δ = 0.58).[75] *Pseudomonas aeruginosa c*–551, with an intra–ligand angle of ~54˚, has a relatively axial EPR spectrum with g_{max} of 3.2 and V/Δ = 0.37 (Figure 3E).[28] However, the axial His and Met orientations for *Bacillus pasteurii* cytochrome *c*–553 are similar to those of the mitochondrial cytochromes *c* (with an intra–ligand angle of ~ 48˚),[76] but the protein exhibits a large g_{max} of 3.36 and V/Δ = 0.31 (Figure 3D).[31] It thus appears that the heme structural factors (including planarity of the heme core and orientation and dynamics of the axial groups) contribute to tune the ligand field in a complicated manner. To assess the mutual orientation (and dynamics) of the axial groups and their impact on heme ligand–field anisotropy, paramagnetic NMR serves as an essential complement to EPR spectroscopy. This technique gives direct information on the spin density distribution (ρ_i^{π}) residing on the porphyrin core and on the magnetic susceptibility anisotropy ($\Delta\chi$) of the system and its axial ($\Delta\chi_{ax}$) and rhombic ($\Delta\chi_{rh}$) components (*vide infra*).[77-80] The heme group in ferricytochromes *c* (S = ½) displays an asymmetric allocation of the unpaired electron spin density among the heme pyrrole *β*–substituents,[81] and this asymmetry can be associated with the orientations of the heme axial ligands, His and Met. Unfortunately, in spite of the large amount of information gained through such analyses, a direct relationship between the magnitudes of axial and rhombic distortions (and thus the EPR *g*–values) versus relative configuration of His/Met ligand and Met dynamics has not been found. Furthermore, from EPR and Mössbauer studies carried out previously on *N. europaea c*–552 and *B. pasteurii c*–553 a pH-dependent conversion between type I and type II EPR species can additionally be present in the systems, rendering their analyses even more complex.[31]

^{1}H NMR ANALYSES OF CYTOCHROME *C* (HIS–MET) PROTEINS

The oxidized ($S = {}^1/_2$) state of cytochromes *c* displays two to four well–resolved hyperfine–shifted resonances of relative intensity 3 which are relatively narrow for paramagnetic molecules and thus can be detected rather easily in 1–D NMR spectra.[82,83] These resonances originate from the methyl groups on the heme macrocycle at positions 1, 3, 5, and 8, (Fisher numbering system) and are shown in Figure 8 for a representative set of cytochrome *c* proteins (*N. europaea c*–552, *P. aeruginosa c*–551and *H. thermophilus c*–552) and their related mutants. The X–ray structures for these proteins are shown in Figure 6 while Figure 7 (A and B) illustrates the positions in which mutations have been induced in *N. europaea c*–552 and *P. aeruginosa c*–551. The shifts of the heme methyls are determined by the heme electronic structure, which is linked to the details of the structure of the heme and its axial ligands. Contributions to the observed shifts (δ_{obs}) are given by Eq. (7)

$$\delta_{obs} = \delta_{dia} + \delta_{para} = \delta_{dia} + \delta_{con} + \delta_{pc} \qquad (7)$$

where δ_{dia} and δ_{para} represent respectively the shift of the nucleus in an isostructural diamagnetic molecule and the contribution to the shift from the unpaired electron–nucleus interaction.[84-86] The term δ_{para} is determined by two contributions: (i) the contact (through–bond, δ_{con}) and pseudocontact (through–space, δ_{pc}) components. Assuming the existence of a single spin state, δ_{con} is described by Eq. (8)[83,84,86]

$$d_{con} = \left(\frac{2pA}{h}\right)\left[\frac{gbS(S+1)}{3kTg}\right] \qquad (8)$$

where $2\pi A/h$ is the hyperfine coupling constant for the nucleus, g is the average g value, β represents the Bohr magneton, γ is the nuclear magnetogyric ratio, S is the total electron spin, k is the Boltzmann constant, and T the absolute temperature. The pseudocontact (or dipolar) contribution, as given by Eq. (9), to the hyperfine shift depends on the position of the nucleus

(in polar coordinates, r, θ, Ω) with respect to the principal axes of the magnetic susceptibility tensor χ and the magnetic anisotropy (axial, $\Delta\chi_{ax}$, and rhombic, $\Delta\chi_{rh}$) of the system[83,86]

$$d_{pc} = (12\pi\mu_0 Nr^3)^{-1}\left[\Delta c_{ax}(3\cos^2\theta - 1) + 3/2\Delta c_{rh}(\sin^2\theta\cos 2\Omega\right] \qquad (9)$$

The contact and pseudocontact shifts are closely related to the type and orientation of the heme axial ligands. Walker and Shokhirev[87] have shown that the heme methyl shift patterns in low–spin ferriheme proteins, which are dominated by δ_{con}, can be related to heme axial ligand orientations via simple Hückel calculations. Pseudocontact shifts are connected to the heme axial ligand orientations via the "counterrotation rule".[75,78] Thus if the mean axial ligand plane is oriented at an angle Φ from a N–Fe–N axis in the heme plane, then the direction of the minimum χ value (χ_{xx}) lies at an angle $\kappa = -\Phi$ from that same axis (Figure 9). Looking at different structural families, cytochromes *c* tends to exhibit different heme methyl shift patterns. Eukaryotic cytochromes *c* typically display a pairwise ordering of heme methyl resonances[88] such that methyls 8 and 3 appear downfield (at ~30–35 ppm) with respect to methyls 5 and 1 (at ~10 ppm) (Figure 8B). In contrast, bacterial cytochromes *c* structurally similar to *Pseudomonas aeruginosa* (Pa) cyt *c*–551 usually display a reversed resonance pattern, with methyls 5 and 1 featuring downfield signals compared to methyls 8 and 3 (Figure 8A).[88] These different fingerprints result from the different orientations of the heme axial Met (*vide infra*). The axial group His in cytochromes *c*, in fact, is structurally more rigid and tends to be constrained along the α–γ–meso axis.[29] The Met orientation found in bacterial cytochrome c_8s and eukaryotic cytochrome cs differ essentially by inversion through the axial Met sulphur. This change in ligand conformation induces alteration of the Met ligand angle of ~56°.[89] The net result is a remarkable modification of the unpaired electron delocalization pattern on the heme macrocycle, being accompanied by a change in the orientation of the

magnetic axes, which is reflected in the pseudocontact shifts.[89,90] Despite the advances made in relating hyperfine shifts to the details of heme–ligand interactions in cytochromes *c*, some of them display ^{1}H NMR properties that cannot be readily understood under this framework. The inability to describe the behaviour of the hyperfine shifts in these proteins brought into question whether models relating heme ligation to electronic structure, and thus NMR spectra, are incomplete, or whether there are aspects of heme–ligand interactions not understood in some of these proteins.[87,91,92] In particular, as shown in Figure 8C and 8D respectively, both cytochrome *c*–552 from *Nitrosomonas europaea* (Ne)[89,92] and cytochrome *c*-552 from *Hydrogenobacter thermophilus* (Ht)[89,91] exhibit anomalous and highly compressed heme methyl shift patterns, not readily interpreted in terms of a single orientation of the His and Met axial ligands. The same is true for a mutant of Ne *c*–552 (NeV65Δ, Figure 8G)[52] and for a mutant of Pa *c*–551 (PaN64Q, Figure 8J).[52,93] Such an effect is now attributed to the ability of the Met axial group to undergo a rapid (on the NMR time scale) change in configuration (stereochemistry at sulphur) and has been referred to in the literature using the term "fluxionality".[82,89,94] The prototypical patterns of heme methyl shifts corresponding to the most frequently observed axial Met orientations are depicted graphically in Figure 8 (left boxes) as conformations A, B and A+B. In what will be referred to herein as orientation A, which is seen in the ^{1}H NMR spectrum of Pa *c*–551 (Figure 8A), the heme axial Met ε–CH_3 is directed toward pyrrole IV. This structural arrangement causes the unpaired electron to be localized more on pyrroles I and III ($3e_g(\pi_y)$) rather than on pyrroles II and IV ($3e_g(\pi_z)$) yielding a heme methyl shift arrangement (δ_{Me}) of 5–CH_3 > 1–CH_3 > 8–CH_3 > 3–CH_3. Orientation B, which is seen in cytochrome *c* from horse heart (Figure 5B), corresponds to the axial Met ε–CH_3 directed toward pyrrole I. This conformation induces the unpaired electron to be localized more on pyrroles II and IV with shift pattern of 8–CH_3 > 3–CH_3 > 5–CH_3 > 1–CH_3. In Ne *c*–552 and Ht *c*–552, the methyl shift spread is unusually small, only 4.2 ppm, indicating nearly

equal unpaired electron spin–density at the four pyrrole groups. The compressed δ_{Me} is consistent with the averaging of the shifts for the two prototypical Met conformations (A+B). However, such compressed pattern itself does not ensure for the presence of a fluxional ligand (see e.g. Figure 8H where NeG50N/V65Δ adopts Met–configuration A) and thus additional evidence is needed to support the occurrence of Met fluxionality. The presence of significant line broadening for the heme methyl resonances as a function of temperature indicates the presence of a chemical exchange process impacting the heme methyl shifts, and thus those properties are usually used to confirm the presence of a fluxional Met. The factors controlling Met fluxionality are as yet uncertain, although the mutation of amino acid residues which interact with the heme axial Met have been shown, as reported in Figure 7, to suppress or even induce Met dynamics, as well as alter Met orientation.[80,93] A suggested hypothesis is that a weak Fe–Met bond combined with a large heme pocket that can accommodate multiple Met orientations results in Met fluxionality. However, as shall we see later on, the presence of Met fluxionality seems irrelevant as to the tuning of the ligand–field anisotropy in the systems.

MODULATION OF THE HEME ANISOTROPY THROUGH SITE DIRECTED MUTAGENESIS

The EPR and ^{1}H NMR analyses performed recently on a series of mutants derived from Pa *c*–551 and Ne *c*–552 disclosed that the ligand–field can be shifted from weakly axial (Pa *c*–551) or moderately axial (Ne *c*–552) to nearly rhombic (PaN64V and NeN64Δ) by modifying the sequence in the loop containing the axial Met.[52] The induced modulation of the ligand–field arises from both steric factors and perturbation of the electrostatic (polar) interaction between the axial ligand Met61 and Asn64 (N64). The residue N64 is structurally located on the axial Met–bearing loop in these proteins (Figure 7) and it has been shown to play an important role

in determining the axial Met conformation relative to the heme for Pa *c*–551. Upon substitution of N64 in Pa *c*–551 with a group having similar polarity but slightly greater bulk such as glutamine residue (PaN64Q) only slightly modifies the original ligand–field witnessed in the wild–type form. The same is true for NeV65Δ, where the axial Met–bearing loop has been shortened by a valine residue. The double mutant NeG50N/V65Δ additionally substitutes the flexible G50 residue at the end of the loop with asparagine, the corresponding residue in Pa *c*–551, in addition to deletion of V65. Because Ne *c*–552 has one more residue in this loop, its greater length was proposed to alter its packing against the heme[5] and this effect might account for the observed Met fluxionality in Ne *c*–552. In the expressed NeG50N/V65Δ double mutant, the Met fluxionality was in fact hindered and adopted configuration A. However, the ligand–field strength did not change and remained essentially moderately axial as in the wild type form. The complementary double mutant of Pa *c*–551 (PaV65ins/N50G) was also prepared together with the PaN64V mutation which replaced the polar asparagine residue with the hydrophobic, isosteric side chain of valine. This mutation provided only a weak shift of the ligand–field towards increased rhombicity. From these studies, it became clear that when Met and His act as axial ligands, even minor electronic perturbations of the Met group are enough to trigger changes in ligand–field anisotropy from (weakly) axial to rhombic. Mutation of the axial Met (e.g. in Ht *c*–552, vide infra) will induce some chances in the type II EPR spectrum as well as formation of a novel high spin ($S = 5/2$) form similar to that seen, for instance, in myoglobin (Figure 10). However, for His/Met–ligated systems, no clear–cut links have been found between the two ground–state electronic configurations for the heme core and axial groups' orientations. In fact, looking at the NMR and EPR results shown in Table 3, there is no direct relationship between the presence of axial Met dynamics and observation of axial EPR spectra, nor between Met orientation (A, B) (Figure 8) and *g*–tensor parameters, in contrast with cytochromes with bis–His axial ligation

for which ligand orientation and *g*–tensor parameters are clearly correlated.[95] On the other hand, as shown in Figure 11, a linear correlation stands between the observed g_{max} values (or their derived ligand–field anisotropy, *V/Δ* ratio) *versus* the averaged heme methyl chemical shift <δ> that can also accommodate the values taken from some other cytochrome *c* proteins. The correlation shows that i) when the g_{max} signal increases, the average methyl chemical shift <δ> increases and ii) when the ligand field anisotropy *V/Δ* increases (from more axial to rhombic), the average methyl chemical shift <δ> decreases. This finding is reminiscent of the linear relationship observed earlier by Walker between g_{max} (or $|g_{zz}|$) and *V/Δ* with A_{zz}, as determined from Mössbauer data.[29] In order to further test this hypothesis, data on the Ht *c*–552 protein (^{1}H NMR, EPR), and from one of its mutants (HtQ64N) has been included here, since this protein share high sequence identity (57%)[91] and structural homology with its mesophilic counterpart Pa *c*–551, as shown by its X–ray structure (Figure 6D). One additional mutant, HtM61A, has been also expressed in order to illustrate the drastic ligand–field changes induced to the heme core when the axial ligand Met is replaced by alanine. The observed low–temperature X–band EPR spectra are depicted together in Figure 10. The over–expressed Ht *c*–552 (Figure 10A) exhibits an EPR envelope where the ligand–field anisotropy is slightly more axial than Pa *c*–551. Here, substitution of the bulkier glutamine (Q64) with an asparagine group (N64), the same residue present in Pa, yielded little change in the electronic properties of the system (Figure 10C). However in HtM61A, when Met is replaced by alanine, the system becomes an admixture of low and high spin species, as shown in Figure 10B. By including these values (Ht *c*–552 over expressed and mutant HtQ64N) in the trend $g_{max} = f$ <δ> depicted in Figure 11, the linear correlation still holds fairly well. However when other combinations of axial heme ligands are considered, such as for example cytochrome *f* (N–terminal amine and His as axial iron ligands) with g_{max} at 3.51 and <δ> at 17.8 ppm, cytochrome b_5 with g_{max} at 3.03 and <δ> at 11.1 ppm (bis His as axial ligands) or MetMbCN

with g_{max} at 3.45 and <δ> at 17.2 ppm (His and CN as axial ligands) these values are much far away from the linear trend reported in Figure 11 (see e.g. Supporting Information file on Ref. 52). It is also interesting to note that within the cytochrome *c* with His-met axial ligation the largest deviations from the linearity are seen for those proteins exhibiting the largest differences in reduction potential ($E^{0'}$) with respect to those usually found in Class I cytochrome *c*, which normally vary from + 0.20 to < 0.35 Volt (versus NHE).[96] Those proteins are *B. pasteurii c*–553 which exhibits a much lower $E^{0'}$ (+ 0.047 V)[97], *R. palustris* c_2 with a larger $E^{0'}$ value (+ 0.350 V and/or + 0.365 V varying on conditions),[98] and *R. rubrum* c_2 (+ 0.310 V).[99] Therefore it is thus anticipated that the potential for NeN64Δ should also be quite different from the over expressed Ne *c*–552 form. Further analyses of how potential relates to electronic structure will aid in linking the variations in electronic structure of His/Met–ligated hemes with function.

CONCLUSION

In this review we described some of our recent studies on bis–His as well as His–Met coordinated low spin hemes These two types of coordination environment for the low spin Fe^{3+} metal ion can generate EPR envelopes characterized by either large g_{max} values and large *g* anisotropy ($g_{max} \geq 3.3$, type I, HALS species) or specie with small g_{max} values and small *g* anisotropy (type II, $g_{max} < 3.2$, rhombic heme). In bis–His coordinated hemes these effects are linked directly to the orientation of the two His groups with respect to each other such that (i) parallel His planes results in rhombic signal and (ii) perpendicular His planes results in HALS signal. The observation of large g_{max} values (3.38 and 3.48) in the cytochrome *b*–558 subunit of succinate:quinone reductase combined with the observation of a near–infrared magnetic circular dichroism charged transfer band at 1600 nm show that the two heme groups adopt in fact bis–His ligation with perpendicular orientation. These studies allowed building a model of the transmembrane helixes with the two His pair sites. The validity of the model was

confirmed later on by crystal structure analyses. The similar bis–His coordination was observed in heme *a* synthase, in both the heme *a* and heme *b*. On the other hand, analyses of literature data complemented by expression of a novel series of cytochrome *c* mutants derived from *Nitrosomonas europaea* (*c*–552), *Pseudomonas aeruginosa* (*c*–551) and *Hydrogenobacter thermophylus* (*c*–552) demonstrated that when Met and His act as axial ligands, unfortunately no direct and simple correlation exists between the large g_{max} value and the mutual orientation of the Met and His axial ligands. Even slight electronic perturbations of the methionine ligand are actually enough to trigger changes in the heme ligand field strength. While the ligand field present in bis–His systems can be made strong enough by the axial groups arrangements to induce $V/\Delta \rightarrow 0$, hence towards the strong axial case ($V \sim 0$, $g_{max} \rightarrow 4$, $g_{mid} \sim g_{min} \rightarrow 0$) as described in the Griffth and Taylor's theory, for the His–Met low spin heme, the larger covalency present in the S–Fe bonds renders these systems at best highly anisotropic ($g_{max} >> g_{mid} > g_{min}$, $V \neq 0$) but not really axial.

FIGURES CAPTIONS

FIGURE 1 Energy diagram of the d–orbitals level for low–spin ferric ion in with $(d_{xy})^2(d_{xz})^2(d_{yz})^1$ orbital occupancy. Note that the iron e_g orbitals are occupied when high spin and intermediate (e.g. S = 3/2) spin states are present in the system.

FIGURE 2 The two prototypical EPR spectra, recorded at cryogenic temperature (T = 10 K) in (A) an axial or type I specie such as Ne c–552 over–expressed form and (B) a rhombic or type II specie such as the NeN64Δ mutant. In (B) the dashed–line represents the spectrum simulation with *g*–tensor parameters given in the drawing. (C) Oxidized (as isolated) cytochrome *b*–CTA from *Bacillus Subtilis*. (D) Oxidized (as isolated) cytochrome *ba*–CTA from *Bacillus Subtilis*.

FIGURE 3 The X–band (~ 9.66 GHz) EPR spectra of (A) *Methylosinus trichosporium* OB3b *c*–554, (B) *Nitrosomonas europaea* Ne *c*–552, (C) mutant NeV65Δ, (D) *Bacillus pasteurii c*–553, (E) *Pseudomonas aruginosa c*–551, (F) mutant PaN64Q, (G) mutant NeN64Δ, (H) mutant PaN64V, (I) *Methylococcus capsulatus* Bath *c*–555. The symbol Δ in the mutant labels indicate deletion of an aminoacid. Note that the spectrum (H) is almost identical to that featured by Horse heart cyt *c* at neutral pH. The protein solutions were prepared in HEPES Buffer (50 mM, pH 7.5) and spectra recorded at T = 10 K, microwave power 1.0 mW, modulation amplitude 0.75 mT, modulation frequency 100 KHz, 55 dB gain, sweep time 168 sec, time constant 82.92 msec; 4–6 scans were accumulated and averaged. The asterisk (*) indicates Cu^{2+} signal as impurity. The symbol Δ indicates the axial term and V the rhombic term according to Griffith and Taylor's formalism.

FIGURE 4 Crystal structure of two bis–His heme proteins. The heme regions shown with key residues and distances of (A) nitrate reductase A from *E. coli* (resolution 1.9 Å, PDB code 1Q16)[100], (B) nitrate reductase A from *E. coli* with PCP bound (resolution 2.0 Å, PDB code 1Y4Z)[66] and (C) Succinate dehydrogenase/quinone reductase from chicken (resolution 1.74 Å, PDB code 2H88)[101]. The figures were made with PyMOL[102].

FIGURE 5 DFT calculation on bis–His heme model with HALS EPR signal in presence of phenol (A) and in absence of phenol (B) (analog for quinol binding site) hydrogen bonded to His–N. The figures demonstrate no unpaired spin density on the phenol. (Model based on the structure with PDB code 1Y4Z[66].)

FIGURE 6 Four crystal structures (X–ray diffraction) and one NMR structure of His–Met cytochromes *c* with rhombic, weak HALS and HALS EPR signals. The heme regions shown with key residues and distances of (A) and (B) cytochrome *c* from horse heart (resolution 1.9 Å, PDB code 1HRC)[103], (C) cytochrome *c*–551 from *Pseudomonas aeruginosa* (resolution 1.6 Å, PDB code 351C)[104], (D) cytochrome *c*–552 from *Hydrogenobacter thermophilus* (resolution 2.0 Å, PDB code 1YNR)[105], (E) cytochrome *c*–553 from *Bacillus pasteurii* (resolution 0.97 Å, PDB code 1C75)[76], (F) cytochrome *c*–552 from *Nitrosomonas europaea* (NMR structure, PDB code 1A56)[106]. The figures were made with PyMOL[102].

FIGURE 7 Structures of Ne c–552 (A) [106] and Pa c–551 (B) [104]. The mutated and deleted residues have been highlighted. The numbering (one–letter code) of Ne have been adjusted to the numbering of Pa, so G50, M61, N64 and V65 correspond to Gly–48, Met–59, Asn–62 and Val–63 in the PDB file. The figures were made with PyMOL[102].

FIGURE 8 Downfield regions of ^{1}H NMR spectra of oxidized (A) recombinant *Pseudomonas aeruginosa* (Pa *c*–551),[89] (B) horse cyt *c*,[107] (C) recombinant *Hydrogenobacter thermophilus* (Ht *c*–552),[89] (D) recombinant *Nitrosomonas europaea* (Ne *c*–552),[82] (E) PaN64V,[52] (F) Ne<u>N64</u>Δ,[52] (G) Ne<u>V65</u>Δ,[52] (H) NeG50N/<u>V65</u>Δ,[52] (I) PaN50G/V65ins,[52] (J) PaN64Q.[93] The symbol Δ indicates deletion of the underlined aminoacid, "ins" indicates an aminoacid insertion. Samples were 2–3 mM protein in 50 mM sodium phosphate buffer, pH 7.0, with 5× molar excess of $K_3[Fe(CN)_6]$, T = 299 K. The heme methyl resonance assignments used the same numbering system indicated in the right part of the panel (enclosed boxes). The structural drawings in the box provide illustration of the heme axial Met orientations observed in cytochrome *c*. The Met side chain is shown in ball–and–stick format, and P indicates propionate group. Other shift patterns also are possible in case of fluxional Met (A+B) and will depend on the conformations sampled by the Met and the chemical shifts in those conformations.

FIGURE 9 Representation of the counter–rotation rule, which states that the effective axial ligand plane angle (Φ) is related to the orientation of the χ_{xx} axis (κ) according to $\kappa = -\Phi$. Here κ and Φ are angles of rotation from the molecular *x*–axis. The Φ and κ values calculated for (A) Pa cyt *c*–551 and (B) horse cyt *c* assuming that Φ is the mean angle of the two ligands are shown using $\kappa = -\Phi$. Calculated values of κ are in general agreement with experimental values. The axial His orientation is shown with a red line, and the axial Met with a light–blue line. The bisector of these angles, the thick magenta line, defines Φ. The κ values predicted on the basis of this mean ligand angle is indicated with a thick green line. Note that the value of κ determined for Ht cyt *c*–552, −47°, is approximately the average of the values in A and B, consistent with the axial Met sampling the conformations in A and B.

FIGURE 10 X–band EPR spectra of (A) Ht *c*–552, (B) HtM61A, and (C) HtQ64N recorded at cryogenic temperature, T = 10 K. The red–dashed lines represent their related simulations. The g–tensor parameters for (A) and (C) are given in Table 3.

FIGURE 11 Correlation between g_{max} values *versus* the average heme methyl chemical shift $<\delta>$ in the over–expressed Ne *c*–552, Pa *c*–551, Ht *c*–552 proteins and their related mutants together with other cytochrome *c* variants. The cytochrome numbering scheme used (1–19) corresponds to that employed in Table 3.

TABLE 1 Properties of heme in succinate:quinone oxidoreductases from various organisms.

TABLE 2 Effect of addition of phenol or inhibitor (PCP) mimicking quinol binding to bis His membrane bound heme through DFT models (Crystal structure was taken from PDB code 1Y4Z[66]), with single point calculation (SP) and after geometry optimisations (Opt). The DFT calculations were performed at the BP86 level[108,109] with the def2–SV(P) basis sets[110] and using the Turbomole 5.9 software package[111].

TABLE 3 The *g*–tensor values, axial (Δ/ξ) and rhombic (V/ξ) ligand–field parameters, the porphyrin methyl chemical shifts (δ) and the reduction potential (E^0) in Pa *c*–551, Ne *c*–552, Ht *c*–552 over–expressed forms and mutants derived from the EPR (T = 10 ±.0.5 K), ^{1}H NMR and voltammetry measurements. Other relevant literature data for similar cytochrome *c* proteins have been included as well. **Table 3. Footnotes:** [a] Data obtained at cryogenic temperatures ($T \leq 10$ K). [b] Data obtained at neutral pH. [c] *g*–tensor and ligand–field data for the dominant HALS (Type I) component only. [d] Major component, neutral pH. [e] From the ^{57}Fe enriched protein (pH = 7) with values obtained by combination of EPR and Mossbauer data. [f] Data obtained at pH = 5.3. [g] This work. The symbol (ξ) indicates the spin–orbit coupling constant (~ 400 cm^{-1}).

FIGURE 1

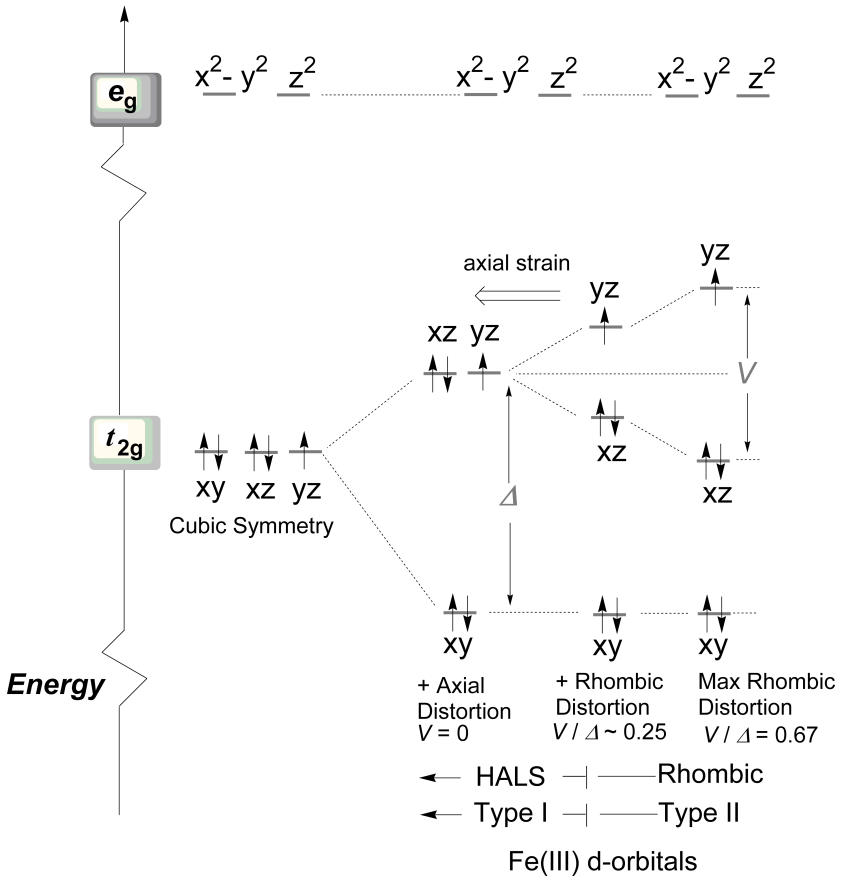
e_g
x^2- y^2 z^2
x^2- y^2 z^2
x^2- y^2 z^2
t_{2g}
xy xz yz
Cubic Symmetry
axial strain
yz
xz yz
V
xz
xz
Δ
xy
xy
xy
Energy
+ Axial Distortion V = 0
+ Rhombic Distortion V / Δ ~ 0.25
Max Rhombic Distortion V / Δ = 0.67
HALS
Rhombic
Type I
Type II
Fe(III) d-orbitals

FIGURE 2

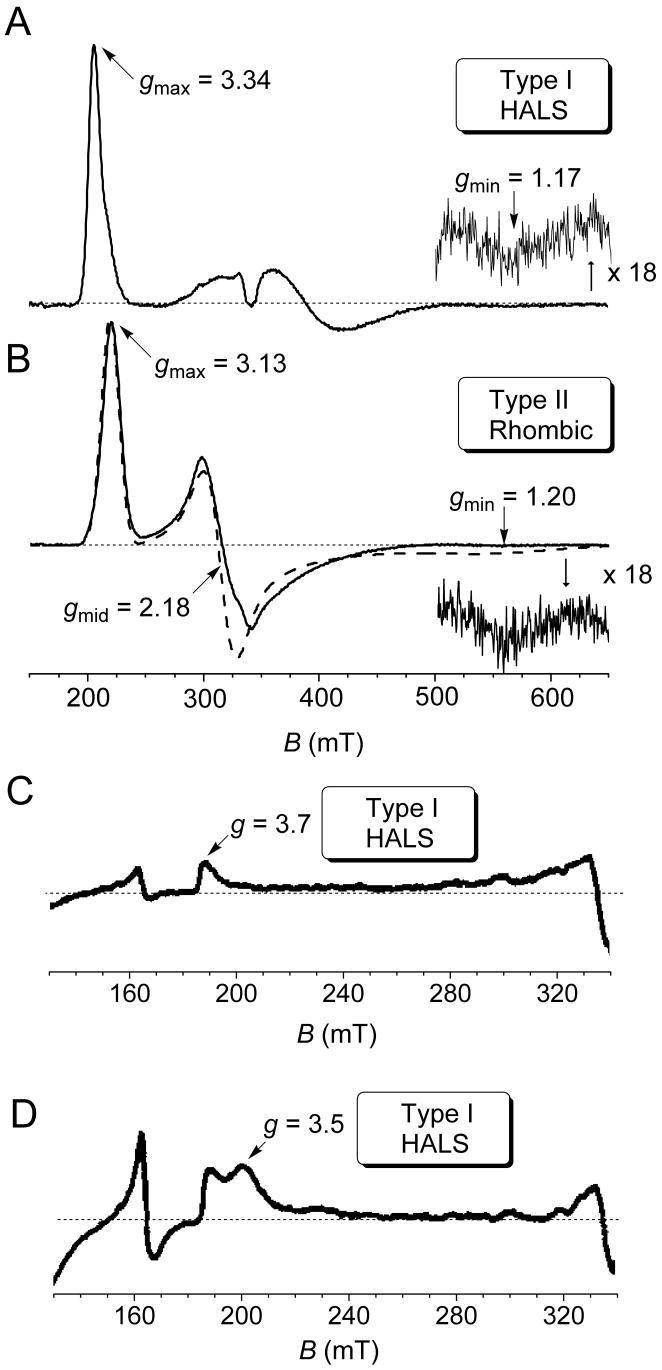
A
g_{max} = 3.34
Type I
HALS
g_{min} = 1.17
x 18
B
g_{max} = 3.13
Type II
Rhombic
g_{min} = 1.20
x 18
g_{mid} = 2.18
200
300
400
500
600
B (mT)
C
g = 3.7
Type I
HALS
160
200
240
280
320
B (mT)
D
g = 3.5
Type I
HALS
160
200
240
280
320
B (mT)

FIGURE 3

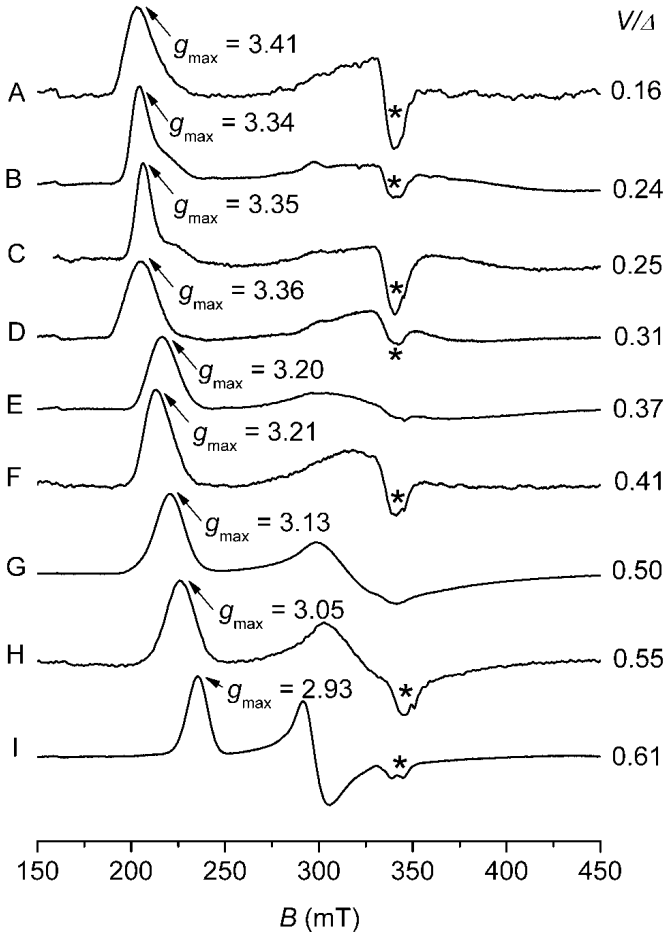
V/Δ
A
B
C
D
E
F
G
H
I
g_{max} = 3.41
g_{max} = 3.34
g_{max} = 3.35
g_{max} = 3.36
g_{max} = 3.20
g_{max} = 3.21
g_{max} = 3.13
g_{max} = 3.05
g_{max} = 2.93
0.16
0.24
0.25
0.31
0.37
0.41
0.50
0.55
0.61
*
150
200
250
300
350
400
450
B (mT)

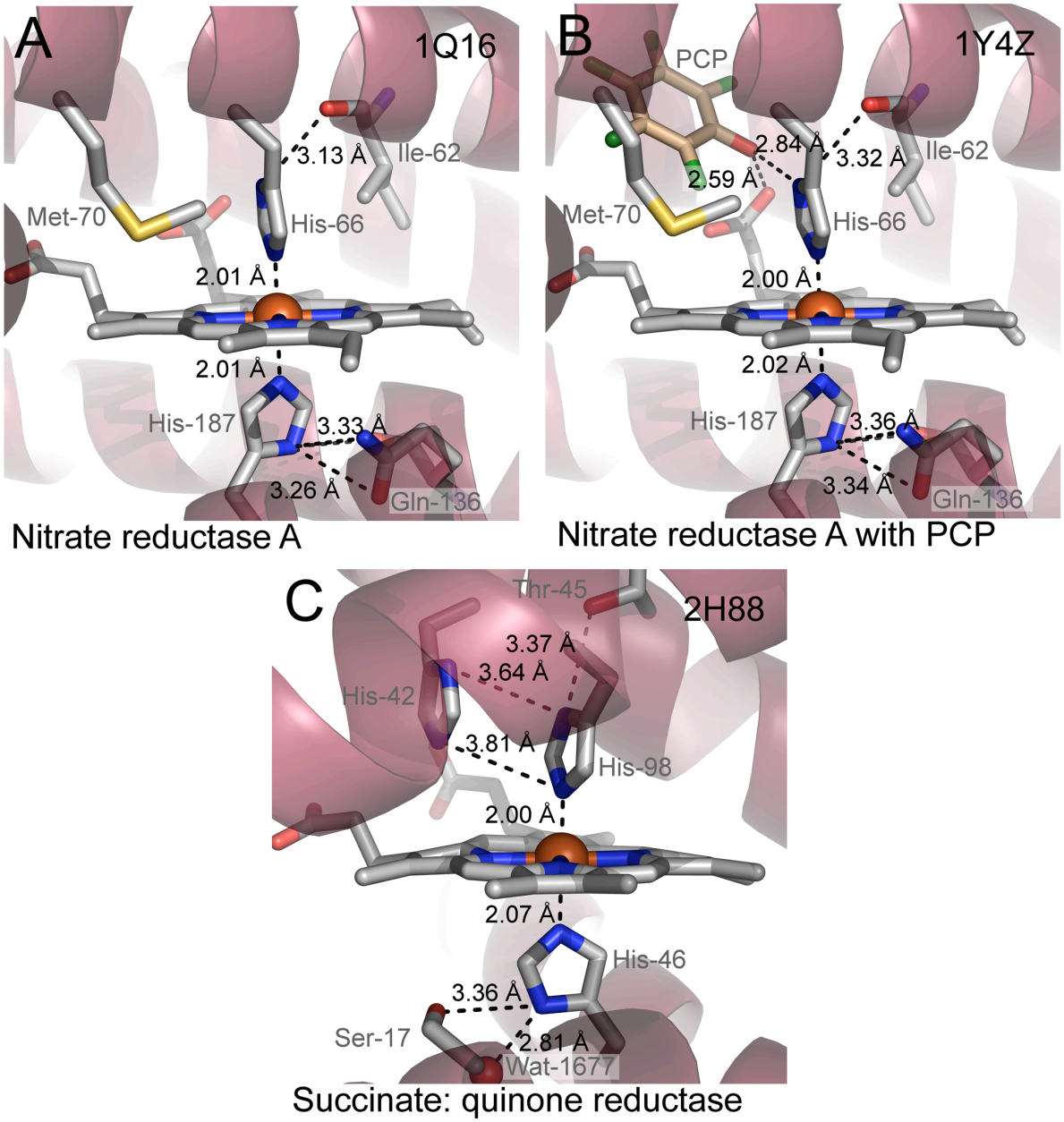
A
1Q16
3.13 Å
Ile-62
Met-70
His-66
2.01 Å
2.01 Å
His-187
3.33 Å
3.26 Å
Gln-136
Nitrate reductase A
B
PCP
1Y4Z
2.84 Å
3.32 Å
Ile-62
2.59 Å
Met-70
His-66
2.00 Å
2.02 Å
His-187
3.36 Å
3.34 Å
Gln-136
Nitrate reductase A with PCP
C
Thr-45
2H88
3.37 Å
3.64 Å
His-42
3.81 Å
His-98
2.00 Å
2.07 Å
His-46
3.36 Å
Ser-17
2.81 Å
Wat-1677
Succinate: quinone reductase

FIGURE 4.

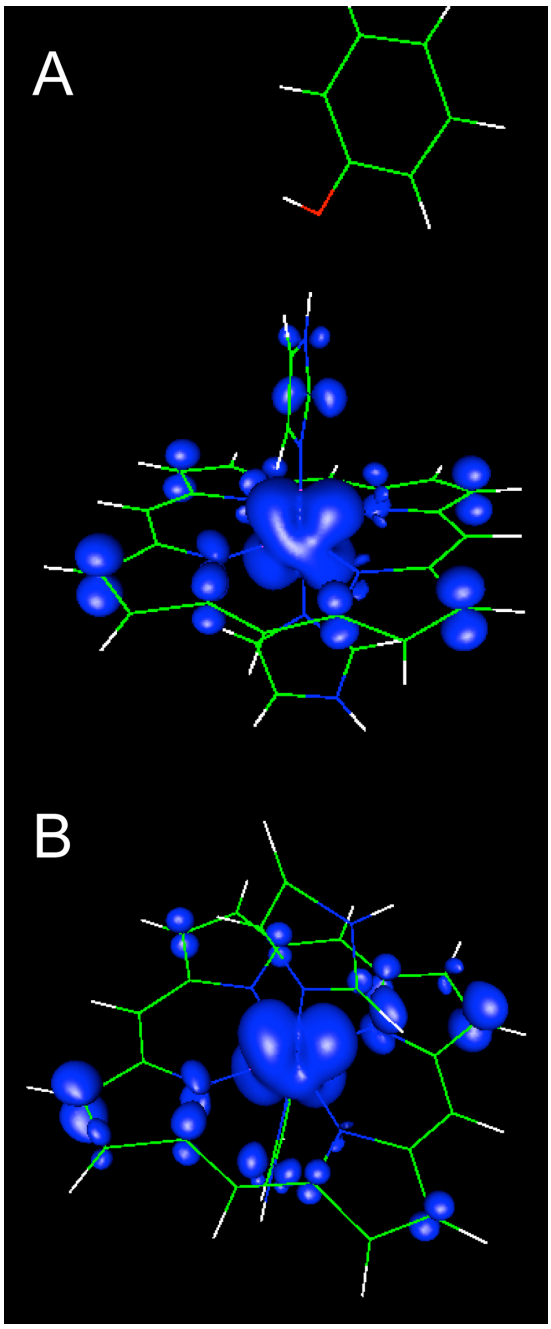

FIGURE 5.

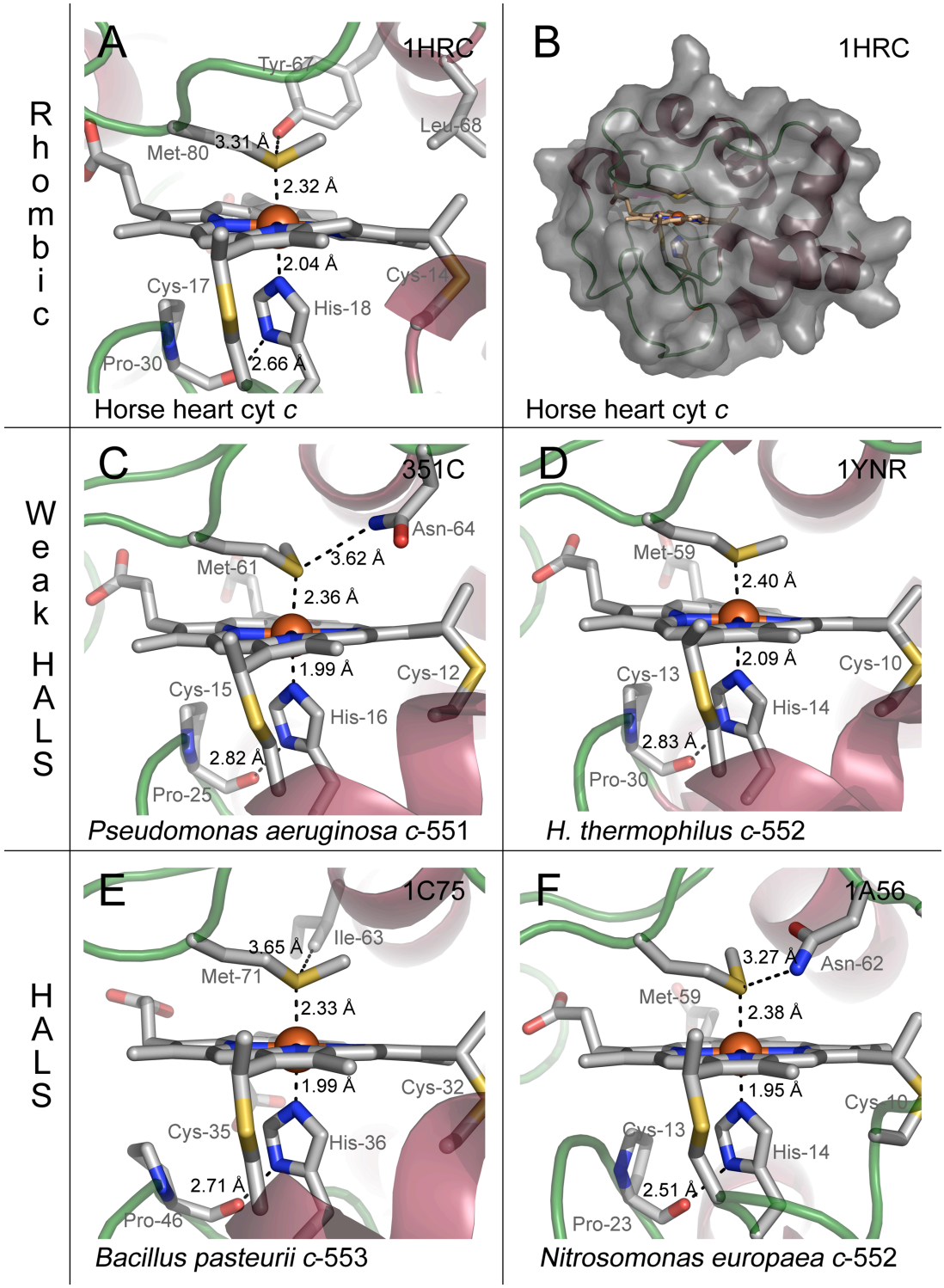
Rhombic
Weak HALS
HALS
A
1HRC
Tyr-67
Leu-68
Met-80
3.31 Å
2.32 Å
2.04 Å
Cys-17
Cys-14
His-18
Pro-30
2.66 Å
Horse heart cyt c
B
1HRC
Horse heart cyt c
C
351C
Asn-64
Met-61
3.62 Å
2.36 Å
1.99 Å
Cys-12
Cys-15
His-16
2.82 Å
Pro-25
Pseudomonas aeruginosa c-551
D
1YNR
Met-59
2.40 Å
2.09 Å
Cys-10
Cys-13
His-14
2.83 Å
Pro-30
H. thermophilus c-552
E
1C75
3.65 Å
Ile-63
Met-71
2.33 Å
1.99 Å
Cys-32
Cys-35
His-36
2.71 Å
Pro-46
Bacillus pasteurii c-553
F
1A56
3.27 Å
Asn-62
Met-59
2.38 Å
1.95 Å
Cys-13
His-14
2.51 Å
Pro-23
Nitrosomonas europaea c-552

FIGURE 6

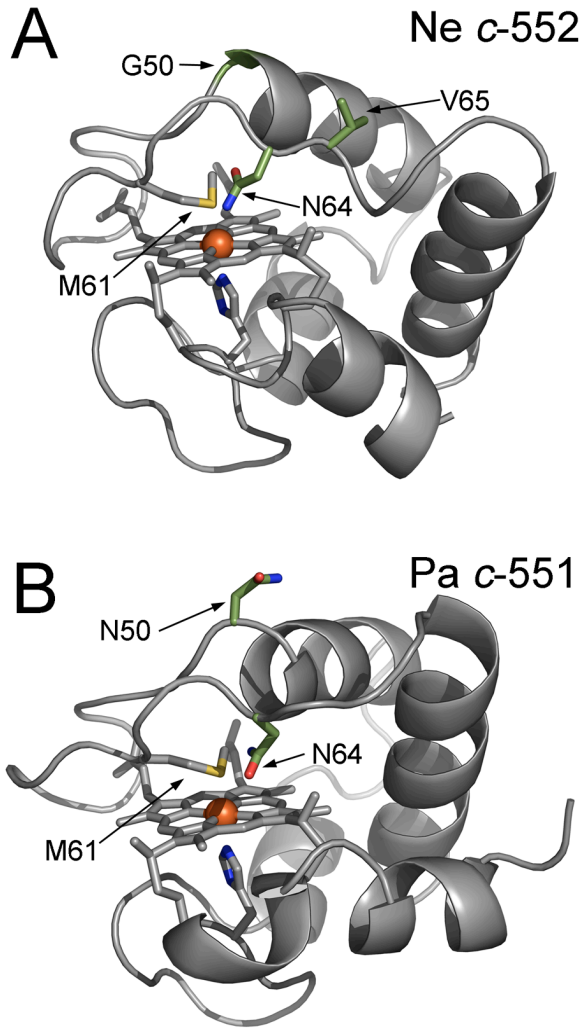

FIGURE 7

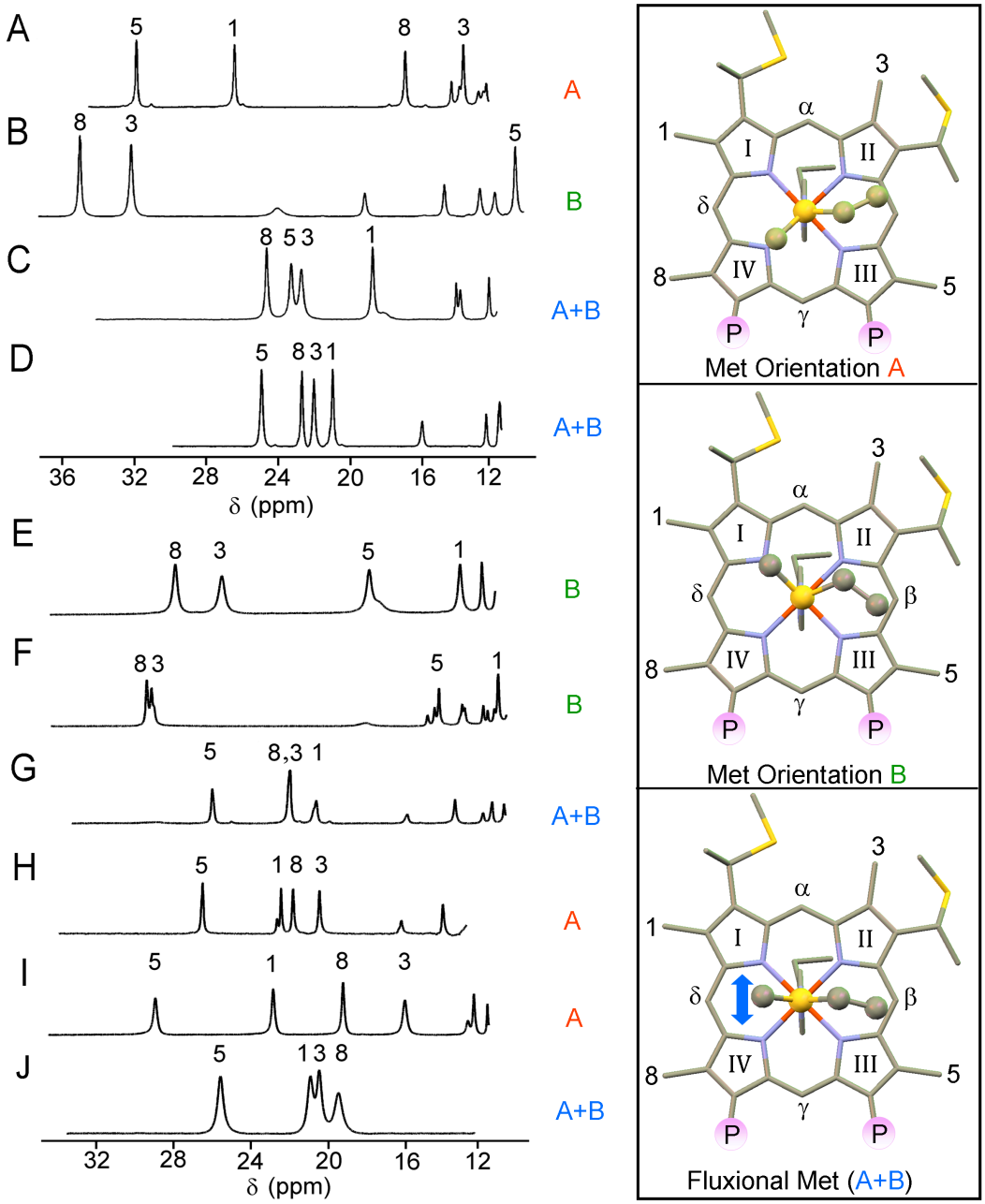
A
5
1
8
3
A
B
8
3
5
B
C
8 5 3
1
A+B
D
5
8 3 1
A+B
36
32
28
24
20
16
12
δ (ppm)
E
8
3
5
1
B
F
8 3
5
1
B
G
5
8,3 1
A+B
H
5
1 8 3
A
I
5
1
8
3
A
J
5
1 3 8
A+B
32
28
24
20
16
12
δ (ppm)
3
α
1
I
II
δ
8
IV
III
5
γ
P
P
Met Orientation A
β
Met Orientation B
Fluxional Met (A+B)

FIGURE 8

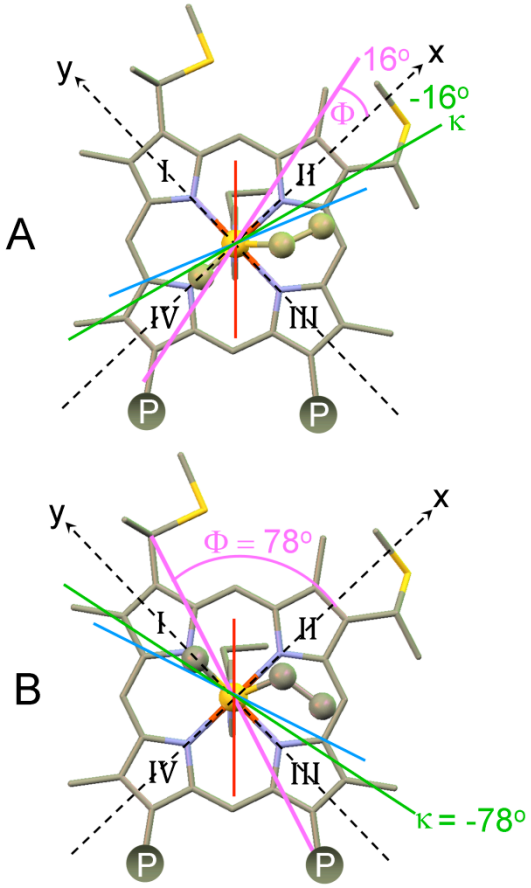

FIGURE 9

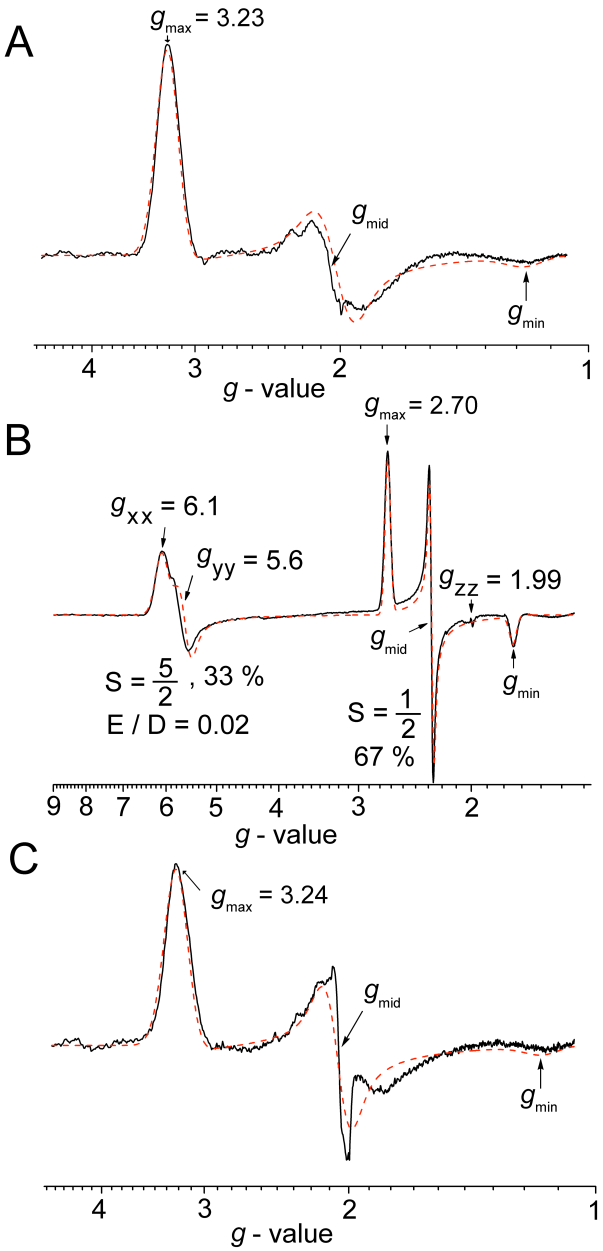
A
g_{max} = 3.23
g_{mid}
g_{min}
4 3 2 1
g - value
B
g_{max} = 2.70
g_{xx} = 6.1
g_{yy} = 5.6
g_{zz} = 1.99
g_{mid}
g_{min}
S = 5/2 , 33 %
E / D = 0.02
S = 1/2
67 %
9 8 7 6 5 4 3 2
g - value
C
g_{max} = 3.24
g_{mid}
g_{min}
4 3 2 1
g - value

FIGURE 10

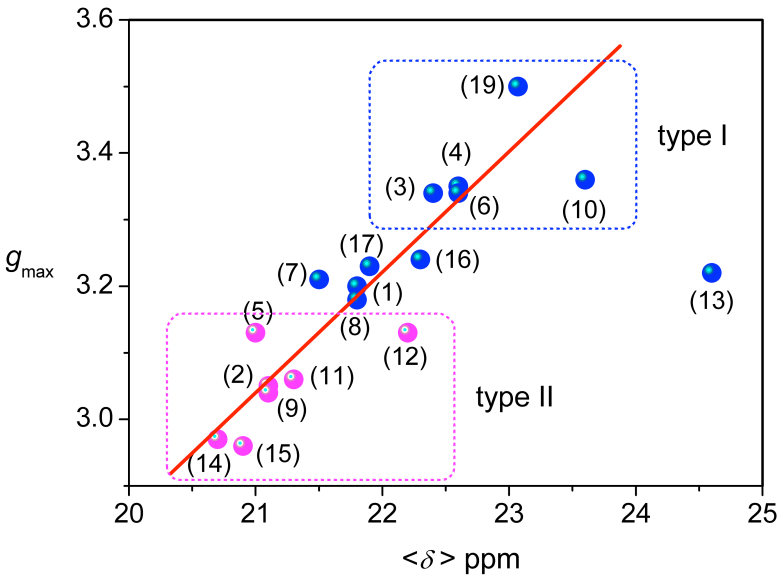
3.6
3.4
3.2
3.0
g_{max}
20
21
22
23
24
25
<δ> ppm
(19)
(4)
(3)
(6)
(10)
type I
(17)
(16)
(7)
(1)
(13)
(5)
(8)
(12)
(2)
(11)
type II
(9)
(14)
(15)

FIGURE 11.

Table 1

Enzyme	No of polypeptides in membrane anchor (TM)[1]	No of hemes	Potential (mV)	EPR spectrum (g_{max})	NIR–MCD	Reference
B. subtilis SQR	1 (5 TM)	2	b_P; +65 b_D; –95	3.68 3.42	1600	[43,56]
W. succinogenes QFR	1 (5 TM)	2	b_H; +20 b_L; –200			[112]
E. coli SQR	2 (3 TM each)	1	+36	3.63	1600	[113,114]
E. coli QFR	2 (3 TM each)	0				
Bovine heart SQR	2 (3 TM each)	1	–185	3.46	1600	[115,116]

[1] TM indicates transmembrane segments

Table 2

	Fe–N distances						Spin density				
No ligand	**NE1**	**NE2**	**NP1**	**NP2**	**NP3**	**NP4**	**Fe**	**Im1**	**Im2**	**Por**	**Phe**
SP	2.00	2.02	1.99	2.02	2.10	2.01	1.03	–0.01	–0.01	0.01	
Opt	2.00	1.99	1.99	2.01	2.00	2.01	1.00	–0.02	–0.01	0.08	
+Phenol SP	2.00	2.02	1.99	2.02	2.10	2.01	1.03	–0.01	–0.01	0.01	0.00
+Phenol Opt	1.98	2.01	2.01	2.00	2.01	2.01	1.01	–0.01	–0.02	0.08	0.00
+PCP SP	2.00	2.02	1.99	2.02	2.10	2.01	0.93	–0.01	–0.02	0.02	0.11
+PCP Opt	1.99	1.99	1.99	2.02	2.00	2.02	0.99	–0.01	–0.01	0.03	0.00

Table 3

Protein variant	g–tensor[a]			Ligand–field			^{1}H NMR methyl shifts, ppm						
His–Met axial ligands	g_{max}	g_{mid}	g_{min}	V/ξ	Δ/ξ	V/Δ	1–CH_3	3–CH_3	5–CH_3	8–CH_3	<δ>	E^0, mVolt[b]	Ref.
(1) *P. aeruginosa c*–551	3.20	2.06	1.23	1.28	3.45	0.37	26.5	13.2	31.5	16.0	21.8	+ 291	[52,117]
(2) *P. aeruginosa* N64V	3.05	2.23	1.31	1.53	2.80	0.55	12.9	25.6	17.7	28.1	21.1	–	[52]
(3) *N. europaea c*–552	3.34	1.87	1.17	1.09	4.45	0.24	20.7	21.6	24.9	22.6	22.4	+ 250	[52,31,117]
(4) *N. europaea* V65Δ[c]	3.35	1.87	1.14	1.06	4.30	0.25	21.9	20.6	26.1	21.9	22.6	+ 232	[117]
(5) *N. europaea* N64Δ	3.13	2.18	1.20	1.36	2.74	0.50	10.9	29.3	14.1	29.7	21.0	–	[52]
(6) *N. europaea* G50N/V65Δ[c]	3.34	1.87	1.15	1.08	4.78	0.23	22.2	20.1	26.4	21.5	22.6	–	[52]
(7) *P. aeruginosa* N64Q	3.21	2.09	1.15	1.23	3.02	0.41	21.4	25.5	19.2	19.8	21.5	+ 250	[52,93,117]
(8) *P. aeruginosa* N50G/V65ins	3.18	2.11	1.26	1.34	3.31	0.40	22.9	15.9	29.3	19.2	21.8	–	[52]
(9) Horse cyt *c*	3.06	2.25	1.25	1.48	2.56	0.58	7.2	31.7	10.2	34.5	21.1	+ 260	[80]
(10) *B. pasteurii c*–553	3.36	1.94	0.98	1.00	3.18	0.31	14.8	28.8	20.9	29.8	23.6	+ 47	[31,97]
(11) *S. cerevisiae* iso–1[d]	3.06	2.25	1.25	1.48	2.56	0.58	8.0	31.3	11.0	34.8	21.3	+ 290	[118,87]
(12) *R. rubrum* c_2 [e]	3.13	2.11	1.23	1.33	3.08	0.43	10.8	29.9	15.0	33.2	22.2	+ 310	[87,30]
(13) *Rh. palustris* c_2	3.22	2.07	1.22	1.27	3.38	0.38	12.4	31.1	18.3	36.4	24.6	≥ + 350	[119]
(14) *P. ZoBell c*–551	2.97	2.24	~1.40	1.69	2.95	0.57	21.2	13.6	30.3	17.6	20.7	+ 250	[87,120]
(15) *P. stutzeri c*–551	2.96	2.27	1.62	2.01	3.86	0.52	21.3	13.7	30.5	18.0	20.9	+ 250–260	[87,121]
(16) *H. thermophilus c*–552	3.23	2.02	1.19	1.22	3.77	0.32	18.2	22.3	22.9	24.3	21.9	+ 215	[82,117,g]
(17) *H. thermophilus* Q64N	3.24	2.06	1.16	1.21	3.51	0.34	26.6	12.9	32.4	17.3	22.3	+ 245	[117,g]
(18) *H. thermophilus* M61A S=1/2 (67%)	2.700	2.305	1.720	–	–	–	–	–	–	–	–	–	[g]
(19) *B. halodenitrificans c*–550[f]	3.50	–	–	–	–	–	26.56	15.55	26.95	23.21	23.07	+ 138	[122,g]

REFERENCES

1. Dolphin, D., Ed. The Porphyrins; Academic Press, Inc.: London, 1979.
2. Bikiel, D. E.; Boechi, L.; Capece, L.; Crespo, A.; De Biase, P. M.; Di Lella, S.; Lebrero, M. C. G.; Marti, M. A.; Nadra, A. D.; Perissinotti, L. L.; Scherlis, D. A.; Estrin, D. A. Phys Chem Chem Phys 2006, 8, 5611–5628.
3. Poulos, T. L.; Li, H. Y.; Raman, C. S. Curr Opin Chem Biol 1999, 3, 131–137.
4. Igarashi, N.; Moriyama, H.; Fujiwara, T.; Fukumori, Y.; Tanaka, N. Nat Struct Biol 1997, 4, 276–284.
5. Hersleth, H. P.; Varnier, A.; Harbitz, E.; Rohr, A. K.; Schmidt, P. P.; Sorlie, M.; Cederkvist, F. H.; Marchal, S.; Gorren, A. C. F.; Mayer, B.; Uchida, T.; Schunemann, V.; Kitagawa, T.; Trautwein, A. X.; Shimizu, T.; Lange, R.; Gorbitz, C. H.; Andersson, K. K. Inorg Chim Acta 2008, 361, 831–843.
6. Hersleth, H. P.; Uchida, T.; Rohr, A. K.; Teschner, T.; Schuenemann, V.; Kitagawa, T.; Trautwein, A. X.; Gorbitz, C. H.; Andersson, K. K. J Biol Chem 2007, 282, 23372–23386.
7. Hersleth, H. P.; Ryde, U.; Rydberg, P.; Gorbitz, C. H.; Andersson, K. K. J Inorg Biochem 2006, 100, 460–476.
8. Lamar, G. N.; Jackson, J. T.; Dugad, L. B.; Cusanovich, M. A.; Bartsch, R. G. J Biol Chem 1990, 265, 16173–16180.
9. Bertini, I.; Gori, G.; Luchinat, C.; Vila, A. J. Biochemistry 1993, 32, 776–783.
10. Margoliash, E.; Schejter, A. Trends Biochem Sci 1984, 9, 364–367.
11. Keilin, D. Proc R Soc Lond B 1925, 98, 312–339.
12. Sigfridsson, E.; Olsson, M. H. M.; Ryde, U. J Phys Chem B 2001, 105, 5546–5552.
13. Blumberg, W. E. Adv Chem Ser 1971, 271–&.
14. Barker, P. D.; Ferguson, S. J. Structure 1999, 7, R281–R290.
15. Allen, J. W. A.; Barker, P. D.; Daltrop, O.; Stevens, J. M.; Tomlinson, E. J.; Sinha, N.; Sambongi, Y.; Ferguson, S. J. Dalton Trans 2005, 3410–3418.
16. Hooper, A. B.; Dispirito, A. A. Microbiol Rev 1985, 49, 140–157.
17. Wood, P. M. FEBS Lett 1983, 164, 223–226.
18. Bowman, S. E. J.; Bren, K. L. Nat Prod Rep 2008, 25, 1118–1130.
19. Berry, E. A.; Walker, F. A. J Biol Inorg Chem 2008, 13, 481–498.
20. Palmer, G. Biochem Soc Trans 1985, 13, 548–560.
21. McGarvey, B. R. Coord Chem Rev 1998, 170, 75–92.
22. Walker, F. A. Chem Rev 2004, 104, 589–615.
23. Griffith, J. S. Proc R Soc Lond A 1956, 235, 23–36.
24. Taylor, C. P. S. Biochim Biophys Acta 1977, 491, 137–149.
25. Alonso, P. J.; Martinez, J. I.; Garcia–Rubio, I. Coord Chem Rev 2007, 251, 12–24.
26. Walker, F. A.; Huynh, B. H.; Scheidt, W. R.; Osvath, S. R. J Am Chem Soc 1986.
27. Scheidt, W. R.; Kirner, J. F.; Hoard, J. L.; Reed, C. A. J Am Chem Soc 1987, 109, 1963–1968.
28. Gadsby, P. M. A.; Thomson, A. J. J Am Chem Soc 1990, 112, 5003–5011.
29. Walker, F. A. Coord Chem Rev 1999, 185–6, 471–534.
30. Huynh, B. H.; Emptage, M. H.; Munck, E. Biochim Biophys Acta 1978, 534, 295–306.
31. Zoppellaro, G.; Teschner, T.; Harbitz, E.; Schuenemann, V.; Karlsen, S.; Arciero, D. M.; Ciurli, S.; Trautwein, A. X.; Hooper, A. B.; Andersson, K. K. Chemphyschem 2006, 7, 1258–1267.

32. Cheesman, M. R.; Greenwood, C.; Thomson, A. J. Adv Inorg Chem 1991, 36, 201–255.
33. Portis, A. M. Phys Rev 1953, 91, 1071–1078.
34. Walker, F. A.; Nasri, H.; TurowskaTyrk, I.; Mohanrao, K.; Watson, C. T.; Shokhirev, N. V.; Debrunner, P. G.; Scheidt, W. R. J Am Chem Soc 1996, 118, 12109–12118.
35. Rivera, M.; Caignan, G. A.; Astashkin, A. V.; Raitsimring, A. M.; Shokhireva, T. K.; Walker, F. A. J Am Chem Soc 2002, 124, 6077–6089.
36. Peisach, J.; Blumberg, W. E.; Adler, A. Ann N Y Acad Sci 1973, 206, 310–327.
37. Devries, S.; Albracht, S. P. J. Biochim Biophys Acta 1979, 546, 334–340.
38. Devries, S.; Albracht, S. P. J.; Leeuwerik, F. J. Biochim Biophys Acta 1979, 546, 316–333.
39. Salerno, J. C. J Biol Chem 1984, 259, 2331–2336.
40. Paul, M. A.; Gadsby, P. M. A.; Thomson, A. J. FEBS Lett 1986, 197, 253–257.
41. Migita, C. T.; Iwaizumi, M. J Am Chem Soc 1981, 103, 4378–4381.
42. Ormejohn.Nr; Hansen, R. E.; Beinert, H. Biochem Biophys Res Commun 1971, 45, 871–878.
43. Friden, H.; Cheesman, M. R.; Hederstedt, L.; Andersson, K. K.; Thomson, A. J. Biochim Biophys Acta 1990, 1041, 207–215.
44. Hederstedt, L.; Andersson, K. K. J Bacteriol 1986, 167, 735–739.
45. Tsai, A. L.; Palmer, G. Biochem Biophys Acta 1982, 681, 484–495.
46. Tsai, A. L.; Palmer, G. Biochim Biophys Acta, 722, 349–363.
47. Schunemann, V.; Trautwein, A. X.; Illerhaus, J.; Haehnel, W. Biochemistry 1999, 38, 8981–8991.
48. Zatsman, A. I.; Zhang, H. M.; Gunderson, W. A.; Cramer, W. A.; Hendrich, M. P. J Am Chem Soc 2006, 128, 14246–14247.
49. Dou, Y.; Admiraal, S. J.; Ikedasaito, M.; Krzywda, S.; Wilkinson, A. J.; Li, T. S.; Olson, J. S.; Prince, R. C.; Pickering, I. J.; George, G. N. J Biol Chem 1995, 270.
50. Arciero, D. M.; Hooper, A. B. J Biol Chem 1994, 269.
51. Arciero, D. M.; Peng, Q. Y.; Peterson, J.; Hooper, A. B. FEBS Lett 1994, 342, 217–220.
52. Zoppellaro, G.; Harbitz, E.; Kaur, R.; Ensign, A. A.; Bren, K. L.; Andersson, K. K. J Am Chem Soc 2008, 130, 15348–15360.
53. Harbitz, E. in preparation.
54. Morris, C., Ed. Academic Press Dictionary of Science and Technology.; Academic Press: San Diego, 2000.
55. Ambler, R. P.; Dalton, H.; Meyer, T. E.; Bartsch, R. G.; Kamen, M. D. Biochem J 1986, 233, 333–337.
56. Hagerhall, C.; Aasa, R.; Vonwachenfeldt, C.; Hederstedt, L. Biochemistry 1992, 31, 7411–7421.
57. Hagerhall, C. Biochim Biophys Acta 1997, 1320, 107–141.
58. Hederstedt, L. Science 1999, 284, 1941–1942.
59. Hagerhall, C.; Hederstedt, L. FEBS Lett 1996, 389, 25–31.
60. Schirawski, J.; Unden, G. Eur J Biochem 1998, 257, 210–215.
61. Schnorpfeil, M.; Janausch, I. G.; Biel, S.; Kroger, A.; Unden, G. Eur J Biochem 2001, 268, 3069–3074.
62. Matsson, M.; Tolstoy, D.; Aasa, R.; Hederstedt, L. Biochemistry 2000, 39, 8617–8624.
63. Smirnova, I. A.; Hagerhall, C.; Konstantinov, A. A.; Hederstedt, L. FEBS Lett 1995, 359, 23–26.

64. Hagerhall, C.; Friden, H.; Aasa, R.; Hederstedt, L. Biochemistry 1995, 34, 11080–11089.
65. Jormakka, M.; Tornroth, S.; Byrne, B.; Iwata, S. Science 2002, 295, 1863–1868.
66. Bertero, M. G.; Rothery, R. A.; Boroumand, N.; Palak, M.; Blasco, F.; Ginet, N.; Weiner, J. H.; Strynadka, N. C. J. J Biol Chem 2005, 280, 14836–14843.
67. Svensson, B.; Andersson, K. K.; Hederstedt, L. Eur J Biochem 1996, 238, 287–295.
68. Mogi, T.; Saiki, K.; Anraku, Y. Mol Microbiol 1994, 14, 391–398.
69. Brown, K. R.; Allan, B. A.; Do, P.; Hegg, E. L. Biochemistry 2002, 41, 10906–10913.
70. Hederstedt, L.; Lewin, A.; Throne–Holst, M. J Bacteriol 2005, 187, 8361–8369.
71. Lewin, A.; Hederstedt, L. FEBS Lett 2006, 580, 5351–5356.
72. Lewin, A.; Hederstedt, L. FEBS Lett 2008, 582, 1330–1334.
73. Ormejohn.Nr; Hansen, R. E.; Beinert, H. J Biol Chem 1974, 249, 1928–1939.
74. Cheesman, M. R.; Kadir, F. H. A.; Albasseet, J.; Almassad, F.; Farrar, J.; Greenwood, C.; Thomson, A. J.; Moore, G. R. Biochem J 1992, 286, 361–367.
75. Shokhirev, N. V.; Walker, F. A. J Am Chem Soc 1998, 120, 981–990.
76. Benini, S.; Gonzalez, A.; Rypniewski, W. R.; Wilson, K. S.; Van Beeumen, J. J.; Ciurli, S. Biochemistry 2000, 39, 13115–13126.
77. Banci, L.; Bertini, I.; Luchinat, C.; Pierattelli, R.; Shokhirev, N. V.; Walker, F. A. J Am Chem Soc 1998, 120, 8472–8479.
78. Turner, D. L. Eur J Biochem 1995, 227, 829–837.
79. Turner, D. L. Eur J Biochem 1993, 211, 563–568.
80. Bertini, I.; Luchinat, C.; Parigi, G. Eur J Inorg Chem 2000, 2473–2480.
81. Walker, F. A. Inorg Chem 2003, 42, 4526–4544.
82. Bren, K. L.; Kellogg, J. A.; Kaur, R.; Wen, X. Inorg Chem 2004, 43, 7934–7944.
83. La Mar, G. N.; Satterlee, J. D.; de Ropp, J. S., Eds.; Academic Press: New York, 2000.
84. Bertini, I.; Luchinat, C.; Aime, S. Coord Chem Rev 1996, 150, R7–+.
85. McConnell, H. M.; Robertson, R. E. J Chem Phys 1958, 29, 1361–1365.
86. Kurland, R. J.; McGarvey, B. R. J Mag Res 1970, 2.
87. Shokhirev, N. V.; Walker, F. A. J Biol Inorg Chem 1998, 3, 581–594.
88. Senn, H.; Wuthrich, K. Quart Rev Biophys 1985, 18, 111–134.
89. Zhong, L. H.; Wen, X.; Rabinowitz, T. M.; Russell, B. S.; Karan, E. F.; Bren, K. L. Proc Natl Acad Sci U S A 2004, 101, 8637–8642.
90. Santos, H.; Turner, D. L. Magn Reson Chem 1993, 31, S90–S95.
91. Karan, E. F.; Russell, B. S.; Bren, K. L. J Biol Inorg Chem 2002, 7, 260–272.
92. Timkovich, R.; Cai, M. L.; Zhang, B. L.; Arciero, D. M.; Hooper, A. B. Eur J Biochem 1994, 226, 159–168.
93. Wen, X.; Bren, K. L. Inorg Chem 2005, 44, 8587–8593.
94. Neese, F. Curr Opin Chem Biol 2003, 7, 125–135.
95. Teschner, T.; Yatsunyk, L.; Schunemann, V.; Paulsen, H.; Winkler, H.; Hu, C. J.; Scheidt, W. R.; Walker, F. A.; Trautwein, A. X. J Am Chem Soc 2006, 128, 1379–1389.
96. Battistuzzi, G.; Borsari, M.; Sola, M. Antioxid Redox Signal 2001, 3, 279–291.
97. Benini, S.; Borsari, M.; Ciurli, S.; Dikiy, A.; Lamborghini, M. J Biol Inorg Chem 1998, 3, 371–382.
98. Geremia, S.; Garau, G.; Vaccari, L.; Sgarra, R.; Viezzoli, M. S.; Calligaris, M.; Randaccio, L. Prot Sci 2002, 11, 6–17.
99. Salemme, F. R. Annu Rev Biochem 1977, 46, 299–329.
100. Bertero, M. G.; Rothery, R. A.; Palak, M.; Hou, C.; Lim, D.; Blasco, F.; Weiner, J. H.; Strynadka, N. C. J. Nat Struct Biol 2003, 10, 681–687.
101. Huang, L. S.; Shen, J. T.; Wang, A. C.; Berry, E. A. Biochim Biophys Acta 2005, 1757, 1073–1083.

102. DeLano, W. L.; DeLano Scientific: San Carlos, CA, USA. http://www.pymol.org, 2002.
103. Bushnell, G. W.; Louie, G. V.; Brayer, G. D. J Mol Biol 1990, 214, 585–595.
104. Matsuura, Y.; Takano, T.; Dickerson, R. E. J Mol Biol 1982, 156, 389–409.
105. Travaglini–Allocatelli, C.; Gianni, S.; Dubey, V. K.; Borgia, A.; Di Matteo, A.; Bonivento, D.; Cutruzzola, F.; Bren, K. L.; Brunori, M. J Biol Chem 2005, 280, 25729–25734.
106. Timkovich, R.; Bergmann, D.; Arciero, D. M.; Hooper, A. B. Biophys J 1998, 75, 1964–1972.
107. Russell, B. S.; Melenkivitz, R.; Bren, K. L. Proc Natl Acad Sci U S A 2000, 97, 8312–8317.
108. Becke, A. D. Phys Rev A 1988, 38, 3098–3100.
109. Perdew, J. P. Phys Rev B 1986, 33, 8822–8824.
110. Weigend, F.; Ahlrichs, R. Phys Chem Chem Phys 2005, 7, 3297–3305.
111. Ahlrichs, R.; Bär, M.; Häser, M.; Horn, H.; Kölmel, C. Chem Phys Lett 1989, 162, 165–169.
112. Unden, G.; Hackenberg, H.; Kroger, A. Biochim Biophys Acta 1980, 591, 275–288.
113. Kita, K.; Vibat, C. R. T.; Meinhardt, S.; Guest, J. R.; Gennis, R. B. J Biol Chem 1989, 264, 2672–2677.
114. Peterson, J.; Vibat, C.; Gennis, R. B. FEBS Lett 1994, 355, 155–156.
115. Crouse, B. R.; Yu, C. A.; Yu, L.; Johnson, M. K. FEBS Lett 1995, 367, 1–4.
116. Yu, L.; Xu, J. X.; Haley, P. E.; Yu, C. A. J Biol Chem 1987, 262, 1137–1143.
117. Ye, T.; Kaur, R.; Wen, X.; Bren, K. L.; Elliott, S. J. Inorg Chem 2005, 44, 8999–9006.
118. Brautigan, D. L.; Feinberg, B. A.; Hoffman, B. M.; Margoliash, E.; Peisach, J.; Blumberg, W. E. J Biol Chem 1977, 252, 574–582.
119. Bertini, I.; Luchinat, C.; Macinai, R.; Martinuzzi, S.; Pierattelli, R.; Viezzoli, M. S. Inorg Chim Acta 1998, 269, 125–134.
120. Cheesman, M. R.; Ferguson, S. J.; Moir, J. W. B.; Richardson, D. J.; Zumft, W. G.; Thomson, A. J. Biochemistry 1997, 36, 16267–16276.
121. van Wonderen, J. H.; Knight, C.; Oganesyan, V. S.; George, S. J.; Zumft, W. G.; Cheesman, M. R. J Biol Chem 2007, 282, 28207–28215.
122. Saraiva, L. M.; Denariaz, G.; Liu, M. Y.; Payne, W. J.; Legall, J.; Moura, I. Eur J Biochem 1992, 204, 1131–1139.